91602
new 82-10

LEGAL NOTICE

This report was prepared by Ontario Hydro and, while effort has been made to assure the accuracy and applicability of the material contained herein, neither Ontario Hydro nor any person acting on its behalf:

(a) makes any warranty, express or implied with respect to the use of any information, apparatus, method or process disclosed in this report or that such use may not infringe privately owned rights; or

(b) assumes any liabilities with respect to the use of, or for damages resulting from the use of, any information, apparatus, method or process disclosed in this report.

ontario hydro
research division

COMPLIMENTARY COPY
Please Credit Ontario Hydro Research if Reproduced in Whole or in Part

# EVALUATION OF CRACKS IN THE LAMBTON TGS UNIT 3 BOILER CIRCULATION PUMP SUCTION MANIFOLD NOZZLES

Report No. 88-199-K

D.A. Scarth
Nondestructive and Fracture Evaluation Section
Metallurgical Research Department

## ABSTRACT

Circumferential cracks have been found in the boiler circulation pump suction manifold nozzles in Lambton TGS Unit 3. The deepest cracks are 20 mm deep. An evaluation of the structural integrity of these cracked nozzles has been completed. The safety margins against fracture initiation and against plastic collapse for the worst case 20 mm deep cracks are 2.66 or greater for normal operating conditions. The safety margins against fracture initiation for the worst case 20 mm deep cracks under hydrostatic test conditions are 1.87 or greater. The cracked nozzles were found to be acceptable for continued service. It was recommended that the cracked nozzles be monitored by means of a periodic inspection program.



| job | file | date | report no. |
|---|---|---|---|
| 83-299-872 | 826.242 | February 22, 1989 | 88-199-K |

ontario hydro
research division

EXECUTIVE SUMMARY

# EVALUATION OF CRACKS IN THE LAMBTON TGS UNIT 3 BOILER CIRCULATION PUMP SUCTION MANIFOLD NOZZLES

Report No. 88-199-K

D.A. Scarth
Nondestructive and Fracture Evaluation Section
Metallurgical Research Department

Circumferential cracks have been detected in the boiler circulation pump suction manifold nozzles in Lambton TGS Unit 3. The cracks lie in the butt-weld regions joining the inlet downcomer nozzles and the outlet pump suction nozzles to the manifold. The deepest cracks are 20 mm deep. An evaluation of the structural integrity of these cracked nozzles has been completed.

Safety margins against fracture initiation, and against plastic collapse were calculated. The safety margins for the worst case 20 mm deep cracks for normal operating conditions are 2.66 or greater. For the hydrostatic test conditions the safety margins against fracture initiation for the 20 mm deep cracks are 1.87 or greater, while the margins against plastic collapse are 6.0 or greater.

The mechanism of crack growth has not been identified. Mechanical fatigue crack growth due to pressure cycles was found to be insignificant. The cracked nozzles were found to be acceptable for continued service. It was recommended that a hydrostatic test be performed on the suction manifold assembly prior to bringing Unit 3 back into service. As well, the cracks should be monitored in the future by means of a periodic inspection program.

| job | file | date | report no. |
|---|---|---|---|
| 83-299-872 | 826.242 | February 22, 1989 | 88-199-K |

TABLE OF CONTENTS


| | | Page |
|---|---|---|
| 1.0 | INTRODUCTION | 1 |
| 2.0 | CONCLUSIONS | 4 |
| 3.0 | RECOMMENDATIONS | 4 |
| 4.0 | MATERIAL PROPERTIES | 4 |
| | 4.1 Tensile Properties | 4 |
| | 4.2 Fracture Toughness $K_{Ic}$ | 5 |
| | 4.3 Thermal Properties | 5 |
| 5.0 | STRESSES | 8 |
| | 5.1 Stresses Due to Mechanical Loads | 8 |
| | 5.1.1 Stage 1 - Loads | 9 |
| | 5.1.2 Stage 2 - Stresses | 9 |
| | 5.2 Thermal Stresses Due to Through-Wall Temperature Gradients | 10 |
| | 5.2.1 Steady-State Thermal Stresses | 10 |
| | 5.2.2 Transient Thermal Stresses | 10 |
| | 5.3 Welding Residual Stress | 11 |
| | 5.4 Total Stresses | 11 |
| | 5.5 Primary Stresses | 11 |
| 6.0 | CRACK-TIP STRESS INTENSITY FACTORS | 20 |
| 7.0 | LIMIT LOAD ANALYSIS | 22 |
| 8.0 | FATIGUE CRACK GROWTH | 22 |
| 9.0 | EVALUATION OF SAFETY MARGINS | 24 |
| | 9.1 Safety Margins on the Crack-Tip Stress Intensity Factor | 24 |
| | 9.2 Safety Margins Against Plastic Collapse | 25 |
| | 9.3 Recommendations | 25 |
| 10.0 | ACKNOWLEDGEMENTS | 25 |
| REFERENCES | | 26 |
| APPENDIX A | | 38 |
| APPENDIX B | | 54 |
| DISTRIBUTION | | last page |

## LIST OF TABLES


Table 4-1 Material Properties

Table 4-2 Fracture Toughness Properties of Lakeview TGS Downcomer Weld Metal From Reference /3/

Table 5-1 Dimensions of Suction Manifold and Nozzles

Table 5-2 Stresses due to Differential Thermal Expansion of the Piping

Table 5-3 Total and Primary Axial Stresses in the Suction Nozzles

Table 5-4 Total and Primary Axial Stresses in the Downcomer Nozzle

Table A-1 Temperatures Used in Piping Thermal Expansion Analyses

Table A-2 Resultant Loads on the Nozzles from the Wardrop Piping Expansion Calculations

Table A-3 Final Loads on Nozzles Used in the Flaw Evaluation

Table A-4 Normalized Membrane and Through-Wall Bending Stresses in the Nozzles

Table A-5 Superposition of Stresses Due to Mechanical Loads for the Suction Nozzle for one Pump Off-Line

Table A-6 Superposition of Stresses Due to Mechanical Loads for the Downcomer Nozzle for One Pump Off-Line

Table B-1 Membrane Stress Geometry Correction Factor for the Axisymmetric Crack

## LIST OF FIGURES


Figure 1-1 Schematic of boiler circulation pump and suction manifold.

Figure 1-2 Schematic illustration of suction manifold nozzles containing cracks in the weld region

Figure 5-1 Schematic of boiler circulation piping system

Figure 5-2 Illustration of membrane and through-wall bending stresses

Figure 5-3 Cold start, load changes and shutdown histories for Lambton TGS Unit 2

Figure 5-4 Illustration of idealized temperature distribution

Figure 6-1 Crack shapes modelled

Figure 9-1 Variation of the margin on the crack-tip stress intensity factor with crack depth for an axisymmetric crack in the suction nozzle for normal operating and design pressures

Figure 9-2 Variation of the margin on the crack-tip stress intensity factor with crack depth for an axisymmetric crack in the suction nozzle for the cooldown transient and the hydrostatic test

Figure 9-3 Variation of the margin on the crack-tip stress intensity factor with crack depth for a crack aspect ratio of 10 to 1 in the suction nozzle for normal operating and design pressures

Figure 9-4 Variation of the margin on the crack-tip stress intensity factor with crack depth for a crack aspect ratio of 10 to 1 in the suction nozzle for the cooldown transient and the hydrostatic test.

Figure 9-5 Variation of the margin on the crack-tip stress intensity factor with crack depth for an axisymmetric crack in the downcomer nozzle for normal operating and design pressures

Figure 9-6 Variation of the margin on the crack-tip stress intensity factor with crack depth for an axisymmetric crack in the downcomer nozzle for the cooldown transient and the hydrostatic test

Figure 9-7 Variation of the margin on the crack-tip stress intensity factor with crack depth for a crack aspect ratio of 10 to 1 in the downcomer nozzle for normal operating and design pressures

Figure 9-8 Variation of the margin on the crack-tip stress intensity factor with crack depth for a crack aspect ratio of 10 to 1 in the downcomer nozzle for the cooldown transient and the hydrostatic test

Figure 9-9 Variation of the margin against plastic collapse with crack depth for an axisymmetric crack in the suction nozzle

Figure 9-10 Variation of the margin against plastic collapse with crack depth for an axisymmetric crack in the downcomer nozzle

Figure A-1 Schematic of lower portion of piping system

Figure A-2 Axial stress distribution through the wall thickness of the suction nozzle weldment used in the flaw evaluation for internal pressure and deadweight

Figure A-3 Axial stress distribution through the wall thickness of the suction nozzle weldment used in the flaw evaluation for piping thermal expansion force - one pump off-line

Figure A-4 Axial stress distribution through the wall thickness of the suction nozzle weldment used in the flaw evaluation for piping thermal expansion bending moments - one pump off-line

Figure A-5 Axial stress distribution through the wall thickness of the downcomer nozzle weldment used in the flaw evaluation for internal pressure and deadweight

Figure A-6 Axial stress distribution through the wall thickness of the downcomer nozzle weldment used in the flaw evaluation for piping thermal expansion force - one pump off-line

Figure A-7 Axial stress distribution through the wall thickness of the downcomer nozzle weldment used in the flaw evaluation for piping thermal expansion moments - one pump off-line

ontario hydro
research division

To

Mr. R.W. Patterson
Manager - Chemistry and
Metallurgy
Central Thermal Services

# EVALUATION OF CRACKS IN THE LAMBTON TGS UNIT 3 BOILER CIRCULATION PUMP SUCTION MANIFOLD NOZZLES

## 1.0 INTRODUCTION

Water in the Lambton TGS boilers is circulated to the bottom of the boiler by means of eight downcomer pipes. A suction manifold is suspended from these downcomers as shown in Figure 1.1. Four circulation pumps, with attached pump motors and eight discharge lines (two for each pump) are suspended from the suction manifold. Cracks have been detected in the pump suction manifold nozzle weld regions in Unit 3. The cracks are inside surface cracks and are orientated circumferentially around the butt-welds joining some of the downcomer nozzles and pump suction nozzles to the suction manifold. A nozzle containing cracks is shown schematically in Figure 1-2. The cracks in the pump suction nozzles are intermittent around 80% of the circumference in the worst case, and range in depths of up to 20 mm. The cracks in the downcomer nozzles are intermittent around the entire circumference of the nozzle, and range in depths of up to 10 mm.

A structural integrity evaluation of these nozzle welds was performed at the request of the Chemistry and Metallurgy Department of Central Thermal Services. This report contains a summary of the evaluation.

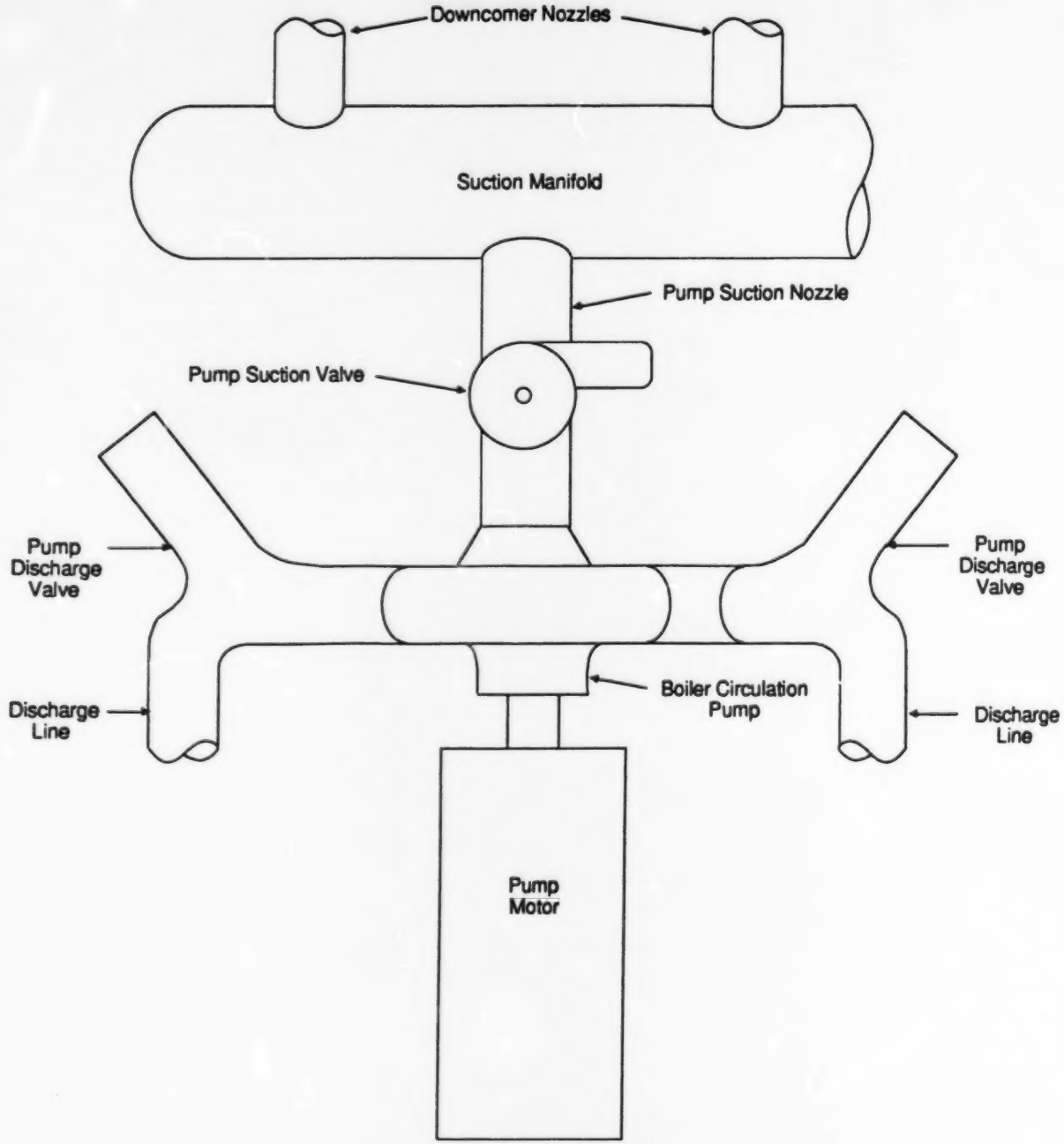


FIGURE 1-1
Schematic of Boiler Circulation Pump
and Suction Manifold

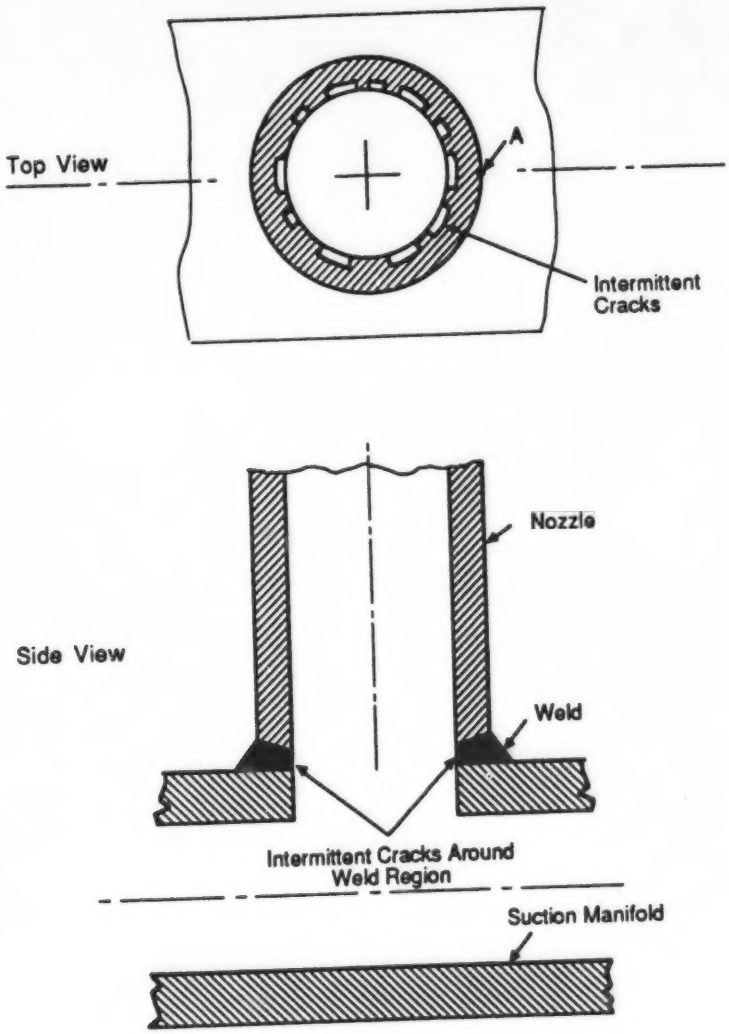


FIGURE 1-2
Schematic Illustration of Suction Manifold
Nozzles Containing Cracks in the Weld Region

## 2.0 CONCLUSIONS

a) An evaluation of the structural integrity of cracks in the circulation pump suction manifold nozzles of Lambton TGS Unit 3 has been completed.

b) The deepest cracks detected were 20 mm deep. Safety margins on the crack-tip stress intensity factor, and against plastic collapse, are greater than 2.66 for the worst case 20 mm deep cracks at normal operating pressures and temperatures.

c) The safety margins on the crack-tip stress intensity factor are 1.87 or greater for the worst case 20 mm deep cracks for the hydrostatic test.

d) The mechanism of crack growth has not been identified. Mechanical fatigue crack growth due to pressure cycles was found to be insignificant.

e) The cracked nozzles are acceptable for continued service. Recommendations are given below.

## 3.0 RECOMMENDATIONS

a) The inspected cracked nozzles are acceptable for continued service.

b) The suction manifold assembly in Unit 3 should be subjected to a hydrostatic test at a pressure of 22.0 MPa and a temperature not less than 25°C.

c) The cracked nozzles should be periodically inspected.

## 4.0 MATERIAL PROPERTIES

Information on the weldments was obtained from CTS. The nozzles and suction manifold were manufactured from A212B carbon steel. The modern day equivalent to A212B is A515 Gr. 70. The welds are shielded metal arc welds and were subjected to post-weld heat treatment.

### 4.1 Tensile Properties

The base metal tensile properties were used. Young's modulus, the yield stress, ultimate stress and flow stress are given in Table 4-1 for the hydrostatic test temperature of 25°C and the design operating temperature of 366°C. The yield and ultimate stresses were taken to be the minimum requirements for A515 Gr. 70 given in ASME Section III, Division 1, Appendix I/1/. The room temperature yield and ultimate stresses are the same as given for A515 Gr. 70 in ASME Section II, Part A (1986). The flow stress was taken to be the average of the yield and ultimate stresses.

## 4.2 Fracture Toughness $K_{Ic}$

The fracture toughness $K_{Ic}$ for this specific weldment is not known. The fracture toughness in the lower-shelf and transition temperature range was taken to be the lower-bound $K_{Ic}$ versus temperature curve given in ASME Section XI Appendix A/2/. This curve is described in the equation

$$K_{Ic} = 36.5 + 3.084 \exp [0.036 (T - RT_{NDT} + 55.6)] \quad (4\text{-}1)$$

where $K_{Ic}$ = fracture toughness in MPa $\sqrt{m}$,

$T$ = temperature in $^{o}C$,

$RT_{NDT}$ = reference nil-ductility transition temperature for the material in $^{o}C$.

A value for $RT_{NDT}$ for this weldment and base metal is not known. Charpy tests were performed on weld metal taken from A212B downcomers in the Lakeview TGS/3/. The value of $RT_{NDT}$ for the weld metal was estimated in/3/ to be $-13^{o}C$. Charpy tests have also been performed on the base metal, weld metal and heat-affected zone of A155 KC70 class 1 welded main steam piping for Pickering B/4/, which is similar to A212B. Values of $RT_{NDT}$ were not determined, but the Charpy tests indicated that the $RT_{NDT}$ for the base metal was higher than that for the weld metal and heat-affected zone. Based on the results in/4/, an $RT_{NDT}$ of $21^{o}C$ was assumed.

The value of $K_{Ic}$ in the upper-shelf temperature range was limited to $K_{Ic}$ = 141 MPa $\sqrt{m}$. This is the lower-bound value for $K_{Ic}$ for carbon steel shielded metal arc welds for the upper-shelf temperature range recommended in the proposed ASME Section XI Appendix Z/5/. Values of fracture toughness were obtained from tests on the Lakeview TGS A212B downcomer weld metal, and are given in Table 4-2. Only the test at $364^{o}C$ resulted in a value for $K_{Ic}$ less than 141 MPa $\sqrt{m}$, in that case $K_{Ic}$ was 117 MPa $\sqrt{m}$. The values of $K_{Ic}$ were determined in that series of tests from J-integral resistance stable crack growth curves by following the 1981 ASTM E813 standard/6/. A re-evaluation of the values for $K_{Ic}$ following the 1987 ASTM E813 standard results in higher values of $K_{Ic}$ for all the tests. In particular, the value of $K_{Ic}$ for the $364^{o}C$ test now becomes 141 MPa $\sqrt{m}$. Therefore, a value of $K_{Ic}$ = 141 MPa $\sqrt{m}$ appears to be a reasonable estimate for the upper-shelf temperature range.

## 4.3 Thermal Properties

The coefficient of thermal expansion $\alpha$, was taken from ASME Section III, Appendix I/1/.

TABLE 4-1

Material Properties

| Property | Temperature | |
|---|---|---|
| | 25°C | 366°C |
| Young's Modulus, E (MPa) | $192 \times 10^3$ | $171 \times 10^3$ |
| Yield Stress, $\sigma_{ys}$ (MPa) | 262 | 189 |
| Flow Stress, $\sigma_f$ (MPa) | 373 | 336 |
| Ultimate Stress, $\sigma_u$ (MPa) | 483 | 483 |
| Fracture Toughness, $K_{Ic}$ (MPa $\sqrt{m}$) | 63 | 141 |
| Coefficient of Thermal Expansion, $\alpha$ (1/°C) | $11.54 \times 10^{-6}$ | $15.51 \times 10^{-6}$ |

TABLE 4-2

Fracture Toughness Properties of Lakeview TGS
Downcomer Weld Metal from Reference /3/

| Temperature ($^{o}$C) | $K_{Ic}$ (MPa $\sqrt{m}$) |
|---|---|
| 20 | 185 |
| 20 | 189 |
| 60 | 197 |
| 60 | 198 |
| 345 | 140 |
| 364 | 117 (141)* |

* - recalculated by following ASTM E813-87.

## 5.0 STRESSES

The stresses used in the evaluation were the stresses normal to the plane of the crack (axial stress in the nozzle) in the uncracked nozzle configurations.

### 5.1 Stresses Due to Mechanical Loads

The stresses were based on three-dimensional elastic finite element calculations. The finite element calculations were performed by Wardrop Engineering Inc. (Winnipeg, Manitoba)/7/ by using the commercial finite element computer code ANSYS. Relevant dimensions are given in Table 5-1. Any local stress raisers due to weld undercuts were not considered. The finite element results of piping loads and stresses were then linearly scaled and combined to account for the pressures and piping temperatures used in the flaw evaluation.

The stress analysis addressed the following loads:

i) Internal pressure - 17.0 MPa, normal operating pressure

- 19.7 MPa, design pressure, equal to the minimum safety valve setting pressure

- 22.0 MPa, hydrostatic test pressure.

ii) Deadweight load on each nozzle - $2.26 \times 10^5$ N.

iii) Motor torque on suction nozzle - $1.65 \times 10^4$ N-m.

iv) Forces and moments due to differential expansion of the piping system.

The calculation of stresses due to mechanical loads was performed in two stages. In Stage 1 the loads on the nozzles were calculated. The deadweight load was calculated by summing the weight of the pump casing, pump motor, discharge lines and water which is supported by each nozzle. The piping differential expansion loads were calculated by performing three-dimensional elastic finite element thermal expansion piping analyses. The commercial computer code ANSYS was used, with the piping system modelled by using the piping and pipe fitting elements. A schematic of the piping system modelled is given in Figure 5-1. Details are given in Appendix A of this report.

Stage 2 involved the application of the loads determined from Stage 1 to a detailed three-dimensional continuum elastic finite element model of the suction manifold with the attached suction and downcomer nozzles. The commercial computer code ANSYS was used. This stage produced the variation of stresses through the wall thickness of the nozzle and around the circumference of the nozzle for each loading condition. Details are also given in Appendix A of this report.

5.1.1 Stage 1 - Loads

In the piping thermal expansion analysis all of the piping except for the waterwall tubes and pump discharge lines was at 365°C (688°F). From field measurements at the Lambton TGS, the temperature of the waterwall tubes was set to 400°C (752°F). The temperature of the pump discharge lines addressed two operating scenarios. The first scenario is that of all four pumps being on-line with all of the discharge lines at the same temperature of 365°C. The stresses due to differential piping expansion in the suction manifold nozzles were calculated for this scenario. The second scenario is that of one of the two middle pumps (pump B or C) being off-line, with colder water in the two discharge lines from that pump. The temperature of a discharge line from an off-line pump has not been measured. The discharge line for an off-line pump is still open to the circulation circuit where the discharge line connects to the lower waterwall drum. A temperature difference between the on-line and off-line discharge lines of 278°C (500°F) was postulated as an upper-bound temperature difference. Due to convective mixing the actual temperature difference is expected to be significantly lower.

5.1.2 Stage 2 - Stresses

The stresses due to the motor torque are insignificant. The low stiffness of the combined 1200 waterwall tubes (44 mm OD), compared with the stiffness of the remainder of the piping (minimum OD = 406 mm), resulted in the stresses in the suction manifold nozzles being insensitive to the differential thermal expansion of the waterwall tubes.

The stresses from the Wardrop calculations for the various loads were scaled and combined by using linear superposition, as detailed in Appendix A of this report. The circumferential location around both nozzle types at which the average axial stress across the wall thickness was maximum was at point A in Figure 1-2. The vertical location was in the weldment, where the wall thickness is greater than in the nozzle. The stress profiles due to each load case are given in Appendix A of the report. Also plotted are the conservative linear idealizations of each profile. The linear stress profiles were then expressed in terms of a membrane stress $\sigma_m$ and a through-wall bending stress $\sigma_b$, as illustrated in Figure 5-2. The through-wall bending stress is positive when in tension on the inside surface. The maximum through-wall stress profile, at point A in Figure 1-2, was then idealized as being axisymmetric around the nozzle. The stresses due to differential thermal expansion of the piping are given in Table 5-2. Terms for the pressure and deadweight stresses are given in Section 5.4. The combined membrane and through-wall bending stresses due to differential thermal expansion of the piping was 35% of the total stresses for a temperature difference between the pump discharge lines of 278°C.

## 5.2 Thermal Stresses Due to Through-Wall Temperature Gradients

### 5.2.1 Steady-State Thermal Stresses

The suction manifold and nozzles are covered by about 50 mm of insulation. A simple steady-state one-dimensional thermal analysis based on concentric cylinders yielded a temperature difference across the wall of only 1.8°C. The heat transfer calculations are not given in this report.

Temperature differences across the wall of a pump discharge valve body have been measured for Unit 2, and are given in Figure 5-3. The negligible temperature difference across the wall thickness during steady state is confirmed in the figure. Therefore, steady-state thermal stresses due to through-wall temperature gradients are insignificant.

### 5.2.2 Transient Thermal Stresses

The plot of the inner and outer wall surface temperatures of the discharge valve body in Figure 5-3 show a maximum temperature difference across the wall during the cooldown transient of about 20°C. The inside wall surface is cooler than the outside wall surface during cooldown, and the thermal stress due to the through-wall temperature gradient would be tension on the inside surface. Since the temperature distribution through the wall is not known, it is assumed that the temperature distribution is linear. Based on the ratio of the wall thickness of the suction nozzle to the wall thickness of the valve body, = 73/64, it was assumed that the maximum temperature difference across the wall thickness of the nozzles during cooldown was 30°C. The pressure at this point in the transient is 8.5 MPa.

The distribution of thermal stress through the wall thickness was taken to be that given for a flat plate under full transverse constraint with a linear through-thickness temperature profile. For the temperature distribution given in Figure 5-4 this is given by/8/

$$\sigma_{th} = \alpha E(\Delta T_1/2)(1-2x/t)/(1-\nu) \qquad (5\text{-}1)$$

where $\alpha$ = coefficient of thermal expansion,

$\Delta T_1$ = temperature difference across the wall thickness,

$x$ = distance from the inside wall,

$t$ = wall thickness.

The thermal stress due to through-wall temperature gradients was written as a membrane component, $\sigma_{thm}$, and a through-wall bending component, $\sigma_{thb}$, where from equation (5-1),

$$\sigma_{thm} = 0$$

$$\sigma_{thb} = 59.5 \text{ MPa} \qquad (5\text{-}2)$$

This thermal stress distribution was assumed to be axisymmetric around the circumference of each nozzle.

## 5.3 Welding Residual Stress

The weld was subjected to post-weld heat treatment. An axisymmetric pure membrane welding residual stress equal to 15% of the room temperature yield stress was estimated at 39.3 MPa. This estimation procedure is recommended by The Welding Institute (Cambridge, England)/9/.

## 5.4 Total Stresses

The total stresses are used as input to the fracture mechanics evaluation. By combining the mechanical, local thermal gradient and welding residual stresses the total axial stresses are written for the suction nozzle as

$$\sigma_m = 1.862\ p + 5.187\ W + \sigma_{expm} + 39.3 \times 10^6\ Pa$$

$$\sigma_b = -15.25\ W + \sigma_{expb} + \sigma_{thb} \qquad (5\text{-}3)$$

and for the downcomer nozzle as

$$\sigma_m = 1.619\ p + 21.97\ W + \sigma_{expm} + 39.3 \times 10^6\ Pa$$

$$\sigma_b = -19.53\ W + \sigma_{expb} + \sigma_{thb} \qquad (5\text{-}4)$$

where $p$ = internal pressure (Pa),

$W$ = deadweight load, = $2.26 \times 10^5$ N,

and $\sigma_{expm}$ and $\sigma_{expb}$ are the respective membrane and through-wall bending stresses due to differential thermal expansion of the piping system. The expansion stresses are given in Table 5-2 for the two scenarios of a temperature difference between the pump discharge lines of 0°C and 278°C (500°F). The thermal stress $\sigma_{thb}$ occurs only during the cooldown transient.

The combined total stresses were calculated for normal operating conditions, design conditions and the cooldown transient, for a temperature difference between the discharge lines of both 0°C and 278°C. Stresses were also calculated for the hydrostatic test. The total stresses for the seven sets of conditions for the suction and downcomer nozzles are given in Tables 5-3 and 5-4 respectively. These stress profiles were idealized to occur around the entire circumference of each nozzle.

## 5.5 Primary Stresses

The primary stresses are used as input to the limit load (net-section plastic collapse) analysis. The primary stresses oppose the external forces on the nozzles, which in this case are the internal pressure, deadweight, and piping differential expansion loads. The membrane stresses due to internal pressure, deadweight and piping differential expansion were included as primary

stresses, but the through-wall bending stresses were not included. This is due to the bending stress being induced by the gross structural discontinuity of the nozzle connection and is self-limiting; the bending stress is not required to maintain equilibrium with the external loads on the nozzle.

The primary stress for the suction nozzle is given as

$$\sigma_{prim} = 1.862\ p + 5.187\ W + \sigma_{expm} \qquad (5\text{-}5)$$

and for the downcomer nozzle as

$$\sigma_{prim} = 1.619\ p + 21.97\ W + \sigma_{expm} \qquad (5\text{-}6)$$

where $\sigma_{expm}$ is given in Table 5-2.

Primary stresses for the suction and downcomer nozzles are given in Tables 5-3 and 5-4 respectively. These values for primary stress were assumed to occur around the entire circumference of the nozzle.

TABLE 5-1

Dimensions of Suction Manifold and Nozzles

| Component | Inner Radius (mm) | Outer Radius (mm) | Wall Thickness (mm) |
|---|---|---|---|
| Suction Manifold | 302 | 394 | 92 |
| Suction Nozzle | 206 | 279 | 73 |
| Downcomer Nozzle | 166 | 229 | 63 |

TABLE 5-2

Stresses Due to Differential Thermal Expansion of the Piping

| Component | System Temperature (°C) | Temperature Difference Between Discharge Lines of Adjacent Pumps (°C) | Expansion Stresses | |
|---|---|---|---|---|
| | | | Membrane, $\sigma_{expm}$ (Pa) | Bending, $\sigma_{expb}$ (Pa) |
| Suction Nozzle | 25 | 0 | 0 | 0 |
| | 366 | 0 (all pumps on-line) | $1.02 \times 10^6$ | $4.26 \times 10^6$ |
| | 366 | 278 (one pump off-line) | $6.22 \times 10^6$ | $30.53 \times 10^6$ |
| Downcomer Nozzle | 25 | 0 | 0 | 0 |
| | 366 | 0 (all pumps on-line) | $7.09 \times 10^6$ | 0 |
| | 366 | 278 (one pump off-line) | $12.27 \times 10^6$ | 0 |

TABLE 5-3

Total and Primary Axial Stresses in the Suction Nozzle

| Operating Condition | Internal Pressure (MPa) | Temperature Difference Between Discharge Lines of Adjacent Pumps ($^{o}$C) | Temperature Difference Across Nozzle Wall ($^{o}$C) | Total Axial Stress (MPa) | | Primary Axial Stress, $\sigma_{prim}$ (MPa) |
|---|---|---|---|---|---|---|
| | | | | Membrane, $\sigma_m$ | Bending, $\sigma_b$ | |
| Normal Operating | 17.0 | 0 | 0 | 73.2 | 0.79 | 33.9 |
| | 17.0 | 278 | 0 | 78.3 | 27.1 | 39.0 |
| Design Pressure | 19.65 | 0 | 0 | 78.1 | 0.79 | 38.8 |
| | 19.65 | 278 | 0 | 83.3 | 27.1 | 44.0 |
| Cooldown Transient | 8.5 | 0 | 30 | 57.4 | 60.3 | 18.1 |
| | 8.5 | 278 | 30 | 62.5 | 86.6 | 23.2 |
| Hydro-static Test | 22.0 | 0 | 0 | 81.4 | -3.5 | 42.1 |

TABLE 5-4

Total and Primary Axial Stresses in the Downcomer Nozzle

| Operating Condition | Internal Pressure (MPa) | Temperature Difference Between Discharge Lines of Adjacent Pumps ($^{o}$C) | Temperature Difference Across Nozzle Wall ($^{o}$C) | Total Axial Stress (MPa) | | Primary Axial Stress, $\sigma_{prim}$ (MPa) |
|---|---|---|---|---|---|---|
| | | | | Membrane, $\sigma_m$ | Bending, $\sigma_b$ | |
| Normal Operating | 17.0 | 0 | 0 | 78.9 | -4.41 | 39.6 |
| | 17.0 | 278 | 0 | 84.1 | -4.41 | 44.8 |
| Design Pressure | 19.65 | 0 | 0 | 83.2 | -4.41 | 43.9 |
| | 19.65 | 278 | 0 | 88.4 | -4.41 | 49.1 |
| Cooldown Transient | 8.5 | 0 | 30 | 65.1 | 55.1 | 25.8 |
| | 8.5 | 278 | 30 | 70.3 | 55.1 | 31.0 |
| Hydro-static Test | 22.0 | 0 | 0 | 79.9 | -4.41 | 40.6 |

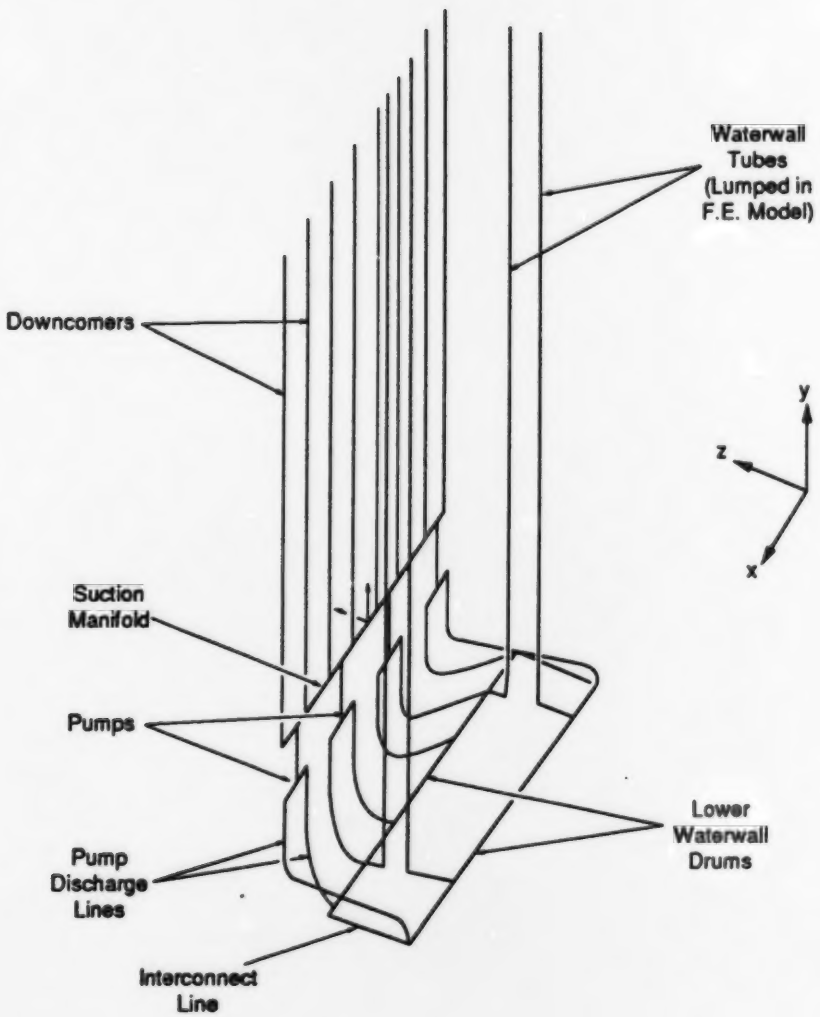


FIGURE 5-1
Schematic of boiler circulation piping system

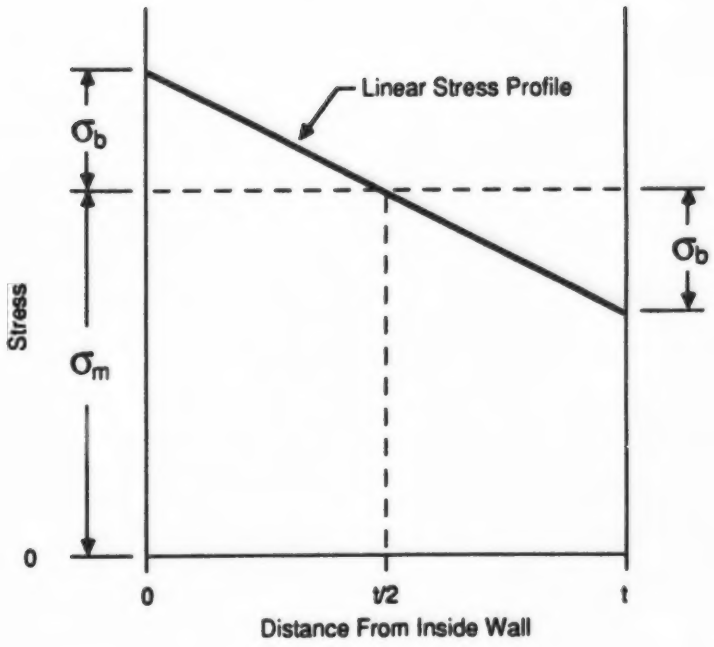


FIGURE 5-2
Illustration of Membrane and Through-Wall
Bending Stresses

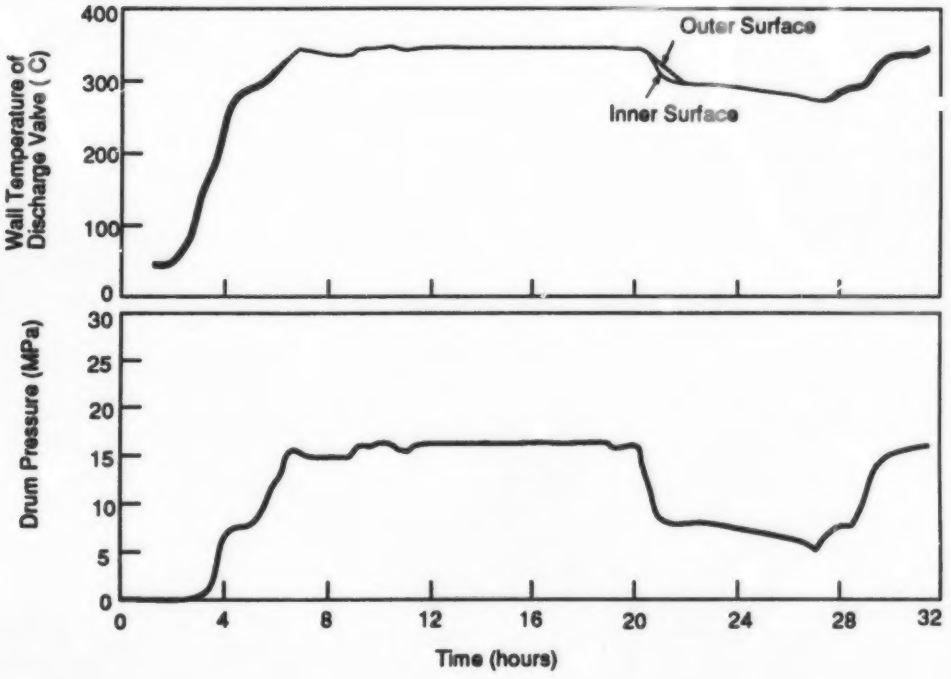


FIGURE 5-3
Cold Start, load changes and shutdown
histories for Lambton TGS Unit 2.

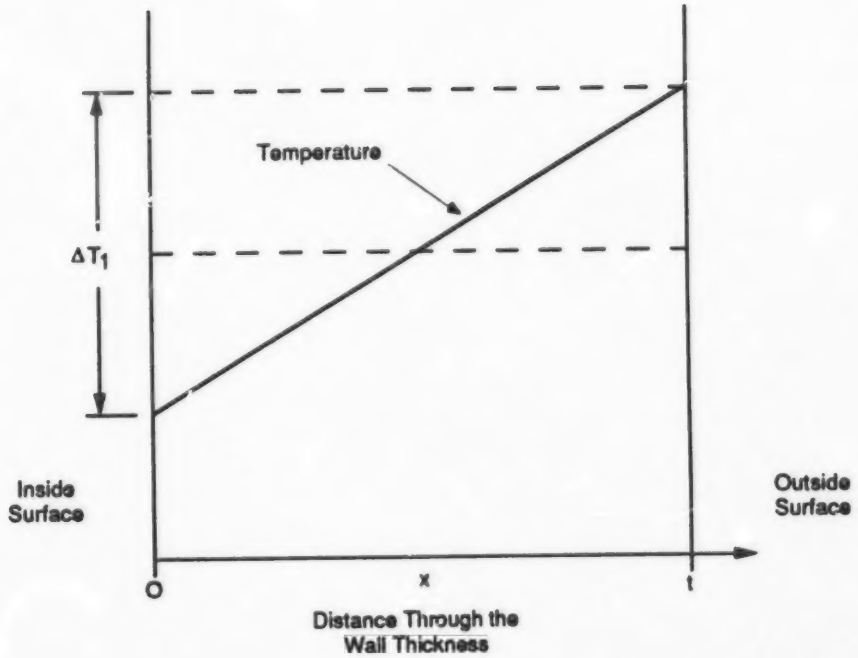


FIGURE 5-4
Illustration of idealized temperature distribution.

## 6.0 CRACK-TIP STRESS INTENSITY FACTORS

The crack-tip stress intensity factor $K_I$ was calculated by following procedures similar to those given in ASME Section XI Appendix A/2/.

$$K_I(a_e) = (\pi a_e/Q)^{0.5} [(\sigma_m + p)F_m + \sigma_b F_b] \quad (6\text{-}1)$$

where $a_e$ - effective crack depth which includes a plastic zone correction,

$$Q = 1 + 1.464 (a/c)^{1.65}, \quad (6\text{-}2)$$

$a$ - actual crack depth

$c$ - one-half the crack length,

$F_m$ - geometry correction factor for the membrane stress, and is a function of $a_e$/wall thickness,

$F_b$ - geometry correction factor for the bending stress, and is a function of $a_e$/wall thickness.

The internal pressure p was added to the membrane stress to account for pressure acting on the crack faces.

The effective crack depth is given by

$$a_e = a + (K_I(a)/\sigma_{ys})^2/(6\pi) \quad (6\text{-}3)$$

where $K_I(a)$ - crack-tip stress intensity factor based on the actual crack depth rather than the effective crack depth,

$\sigma_{ys}$ - yield stress.

Two crack shapes were modelled; an axisymmetric 360° circumferential crack; and a semi-elliptical circumferential crack with a length to depth aspect ratio of 10 to 1. The two crack shapes are shown in Figure 6-1. The geometry correction factors $F_m$ and $F_b$ for each crack shape are given in Appendix B of this report. In the case of the semi-elliptical cracks, the crack-tip stress intensity factor was always maximum at the deepest point of crack penetration.

The safety margin on the crack-tip stress intensity factor is given by the ratio

$$SMK = K_{Ic}/K_I \quad (6\text{-}4)$$

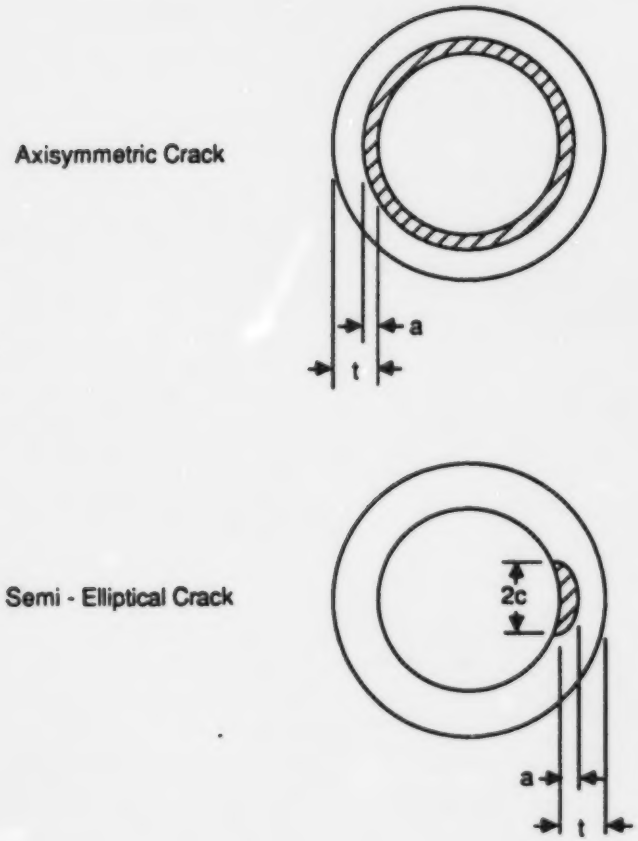


FIGURE 6-1
Crack Shapes Modelled

## 7.0 LIMIT LOAD ANALYSIS

Limit load analysis addresses the possibility of failure of the component by plastic collapse of the remaining ligament prior to failure by fracture. Only the primary stresses, which oppose the external forces on the nozzles (in this case internal pressure, deadweight and differential piping thermal expansion loads) are included in the applied loads. The expression for the limit load $P_{lim}$ of a cylinder under tension containing an axisymmetric crack on the inside surface is given in /10/ as

$$P_{lim} = (2/\sqrt{3})\ \sigma_f\ \pi(R_o^2 - R_c^2) \qquad (7\text{-}1)$$

where $\sigma_f$ = the material's flow stress,

$R_o$ = the outer radius of the nozzle,

$R_c$ = $R_i + a$

$R_i$ = the inner radius of the nozzle.

The total primary load on the net ligament, $P_{net}$, consists of the primary stress $\sigma_{prim}$, idealized to be axisymmetric, plus the load due to pressure acting on the crack faces.

$$P_{net} = \pi[\sigma_{prim}\ (R_o^2 - R_i^2) + p(R_c^2 - R_i^2)] \qquad (7\text{-}2)$$

The margin against plastic collapse is written as

$$SMP = P_{lim} / P_{net} \qquad (7\text{-}3)$$

where $\sigma_{prim}$ is given in Tables 5-3 and 5-4.

## 8.0 FATIGUE CRACK GROWTH

Following ASME Section XI Appendix A/2/, the Paris Rule was used to predict sub-critical crack growth due to mechanical fatigue. The fatigue crack growth rate da/dN is given by

$$da/dN = C_1\ \Delta K_I^{\,n} \qquad (8\text{-}1)$$

where $\Delta K_I$ = range in the crack-tip stress intensity factor over the load cycle,

$$\Delta K_I = K_{Imax} - K_{Imin}, \qquad (8\text{-}2)$$

$K_{Imin}$ = the minimum value of $K_I$ for the cycle,

$K_{Imax}$ = the maximum value of $K_I$ for the cycle,

$C_1$,n are material property fatigue growth rate parameters which are a function of $\Delta K_I$ and the R-ratio, where

$$R = K_{Imin}/K_{Imax}. \quad (8\text{-}3)$$

The range $\Delta K_I$ for the 20 mm deep axisymmetric crack in the suction nozzle is higher than that for the 10 mm deep axisymmetric crack in the downcomer nozzle. The largest range in $\Delta K_I$ is between the shutdown state and the cool-down portion of the startup/shutdown cycle. The fatigue crack growth rate was calculated for the two operating scenarios of: all pumps on-line; one pump off-line with the temperature difference between pump discharge lines postulated to be 278°C. The results are given in Table 8-1. The growth rate properties were taken from ASME Section XI, Appendix A /2/.

Unit 3 has undergone approximately 800 startup/shutdown cycles during the first 19 years of operation. The mechanical fatigue crack growth rate is estimated at 0.00178 mm per cycle for all pumps on-line, and 0.00295 mm per cycle for one pump off-line with a postulated 278° discharge line temperature difference. The accumulated crack growth at these rates for 800 cycles is 1.42 mm and 2.36 mm respectively. Therefore the growth of the cracks to the current depth of 20 mm involved other mechanisms in addition to mechanical fatigue crack growth.

TABLE 8-1

Fatigue Crack Growth Rates for the Suction Nozzle

| Quantity | All Pumps On-line | One Pump Off-line, Temperature Difference Between Discharge Lines Postulated at 278°C. |
|---|---|---|
| $K_{Imin}$ (MPa $\sqrt{m}$) | 12.2 | 12.2 |
| $K_{Imax}$ (MPa $\sqrt{m}$) | 41.2 | 53.0 |
| $\Delta K_I$ (MPa $\sqrt{m}$) | 29.0 | 40.8 |
| R-ratio | 0.2967 | 0.2306 |
| $C_1$ (mm/cycle for $\Delta K_I$ in MPa $\sqrt{m}$) | $2.503 \times 10^{-6}$ | $2.134 \times 10^{-6}$ |
| Growth per cycle (mm) | 0.00178 | 0.00295 |
| Growth in 800 cycles at same growth rate (mm) | 1.42 | 2.36 |

## 9.0 EVALUATION OF SAFETY MARGINS

### 9.1 Safety Margins on the Crack-Tip Stress Intensity Factor

Safety margins on the crack-tip stress intensity factor were calculated using equation (6-4) as a function of crack depth for the seven sets of conditions given in Tables 5-3 and 5-4. These include the following system pressures and temperatures:

| | | |
|---|---|---|
| cooldown transient | - | pressure = 8.5 MPa |
| | - | temperature = 325°C |
| normal operating | - | pressure = 17.0 MPa |
| | - | temperature = 366°C |
| design conditions, minimum safety valve setting | - | pressure = 19.7 MPa |
| | - | temperature = 366°C |
| hydrostatic test | - | pressure = 22.0 MPa |
| | - | temperature = 25°C |

A summary of the minimum safety margins for the deepest crack in a suction nozzle (20 mm) and the deepest crack in a downcomer nozzle (10 mm) is given in Table 9-1.

The minimum safety margin for all conditions except for the hydrostatic test is 2.66, and corresponds to fracture initiation. The minimum safety margin for the hydrostatic test is 1.87, and also corresponds to fracture initiation.

The resulting curves of safety margin for various crack depths for the suction nozzle for the axisymmetric crack are given in Figures 9-1 and 9-2, and for the semi-elliptical crack with an aspect ratio of 10 to 1 in Figures 9-3 and 9-4. The curves for the downcomer nozzle for the axisymmetric crack are given in Figures 9-5 and 9-6, and for the semi-elliptical crack with an aspect ratio of 10 to 1 in Figures 9-7 and 9-8.

The hydrostatic test pressure is 1.3 times the normal operating pressure. The purpose of a hydrostatic test is to proof test the vessel under stress conditions much more severe than normal operating conditions. The procedures used to estimate the safety margins are considered to be conservative. Therefore, sufficient margin exists for the hydrostatic test that no further damage to the nozzles should occur during the test.

The fatigue crack growth analysis has predicted that fatigue crack growth due to mechanical loads following ASME Section XI is not the major cause of the growth of these cracks. The complete mechanism for the growth of these cracks has not been identified. The growth may be due to a corrosion related fatigue mechanism. Therefore, the cracks should be monitored in the future by means of a periodic inspection program.

## 9.2 Safety Margins Against Plastic Collapse

The safety margins against plastic collapse were calculated as a function of crack depth for the axisymmetric cracks using equation (7-3) for the same pressure/temperature states given in Tables 5-3 and 5-4, and listed above. The margins for the cooldown transient (pressure = 8.5 MPa) were the highest, and are not shown. The resulting curves for the suction and downcomer nozzles are given in Figures 9-9 and 9-10, respectively. The margins are 6.0 or greater for the deepest cracks detected in both nozzles, which exceed the safety margins on the crack-tip stress intensity factor.

## 9.3 Recommendations

a) The inspected cracked nozzles are acceptable for continued service.

b) The suction manifold assembly in Unit 3 should be subjected to a hydrostatic test at a pressure of 22.0 MPa and a temperature not less than 25°C.

c) The cracked nozzles should be periodically inspected.

## 10.0 ACKNOWLEDGEMENTS

The author wishes to acknowledge Mr. D.M. Kawa, Mr. J. Hildebrandt and Mr. D. Vanderwees of Wardrop Engineering Inc. for their efforts in carrying out the finite element analyses under the demanding time constraints. The author also acknowledges the assistance of Mr. R.L. McQueen and Dr. D. Sidey of the Chemistry and Metallurgy Department of CTS.

Approved:

J. Brown
for Manager
Metallurgical Research Dept

Prepared:

D.A. Scarth
Engineer
Nondestructive and Fracture
Evaluation Section

Recommended:

B. Mukherjee
Acting Section Head
Nondestructive and Fracture
Evaluation Section

DAS:SEHG:fc

REFERENCES


1. ASME Boiler and Pressure Vessel Code, Section III, Division 1, Appendix I, 1980.

2. ASME Boiler and Pressure Vessel Code, Section XI, 1983.

3. Memo from O. Lepik, Metallurgical Research Dept., to P. Ford and D. Sidey, Chemistry and Metallurgy Dept., CTS, "Fracture Properties of Downcomer Weld of Lakeview TGS, Unit 5", File No. 826.242(T), May 12, 1987.

4. Bellamy, G., "Properties of 28" Diameter Longitudinally Welded Main Steam Piping - Pickering B NGS", Metallurgical Research Dept., Report No. B79-211-H, File No. 823.45, October 11, 1979.

5. "Evaluation of Flaws in Ferritic Piping", proposed Appendix Z to the ASME Boiler and Pressure Vessel Code, Section XI, prepared by the ASME Section XI Task Group on Pipe Flaw Evaluation, January, 1988.

6. "Standard Test Method for $J_{Ic}$, a Measure of Fracture Toughness", American Society for Testing and Materials (ASTM) Standard E813-81, 1981.

7. Letter from D.M. Kawa, Wardrop Engineering Inc. (77 Main St., Winnipeg, Manitoba) to D.A. Scarth, Metallurgical Research Department, "Lambton Thermal Stress Analysis Results", November 16, 1988; plus working notes sent from Wardrop to D.A. Scarth.

8. Timoshenko, S.P. and Goodier, J.N., "Theory of Elasticity", Third Edition, McGraw-Hill, 1970.

9. Garwood, S.J., Willoughby, A.A., Leggat, R.H. and Jutla, T., "Crack Tip Opening Displacement (CTOD) Methods for Fracture Mechanics Assessments: Proposals for Revisions to PD 6493", The Welding Institute, Cambridge, U.K.

10. Kumar, V., German, M.D. and Shih, C.F., "An Engineering Approach for Elastic-Plastic Fracture Analysis", EPRI Report NP-1931, July, 1981.

11. Tada, H., Paris, P.C. and Irwin, G.R., "The Stress Analysis of Cracks Handbook", Del Research Corp., St. Louis, MO., 1973.

12. Zahoor, A., "Closed Form Expressions for Fracture Mechanics Analysis of Cracked Pipes", ASME Journal of Pressure Vessel Technology, Vol. 107, May, 1985, pp 203-205.

13. Newman, J.C. and Raju, I.S., "An Empirical Stress Intensity Factor Equation for the Surface Crack", Engineering Fracture Mechanics, Vol. 15, No. 1-2, 1981, pp 185-192.

TABLE 9-1

Minimum Safety Margins for the Pump Suction Manifold Nozzles

| Description | Margin On Fracture Initiation | | Margin On Plastic Collapse | |
|---|---|---|---|---|
| | Cooldown, Pressure = 8.5 MPa | Hydrostatic Test, Pressure = 22 MPa | Normal Op., Pressure = 17 MPa | Hydrostatic Test, Pressure = 22 MPa |
| Suction Nozzle-Crack Depth = 20 mm | | | | |
| Crack Length/ Depth Aspect Ratio: | | | | |
| Infinite | 2.66 | 1.87 | 6.78 | 6.84 |
| 10 to 1 | 3.73 | 2.30 | - | - |
| Downcomer Nozzle-Crack Depth = 10 mm | | | | |
| Crack Length/ Depth Aspect Ratio: | | | | |
| Infinite | 4.97 | 2.98 | 7.09 | 8.49 |
| 10 to 1 | 5.92 | 3.47 | - | - |

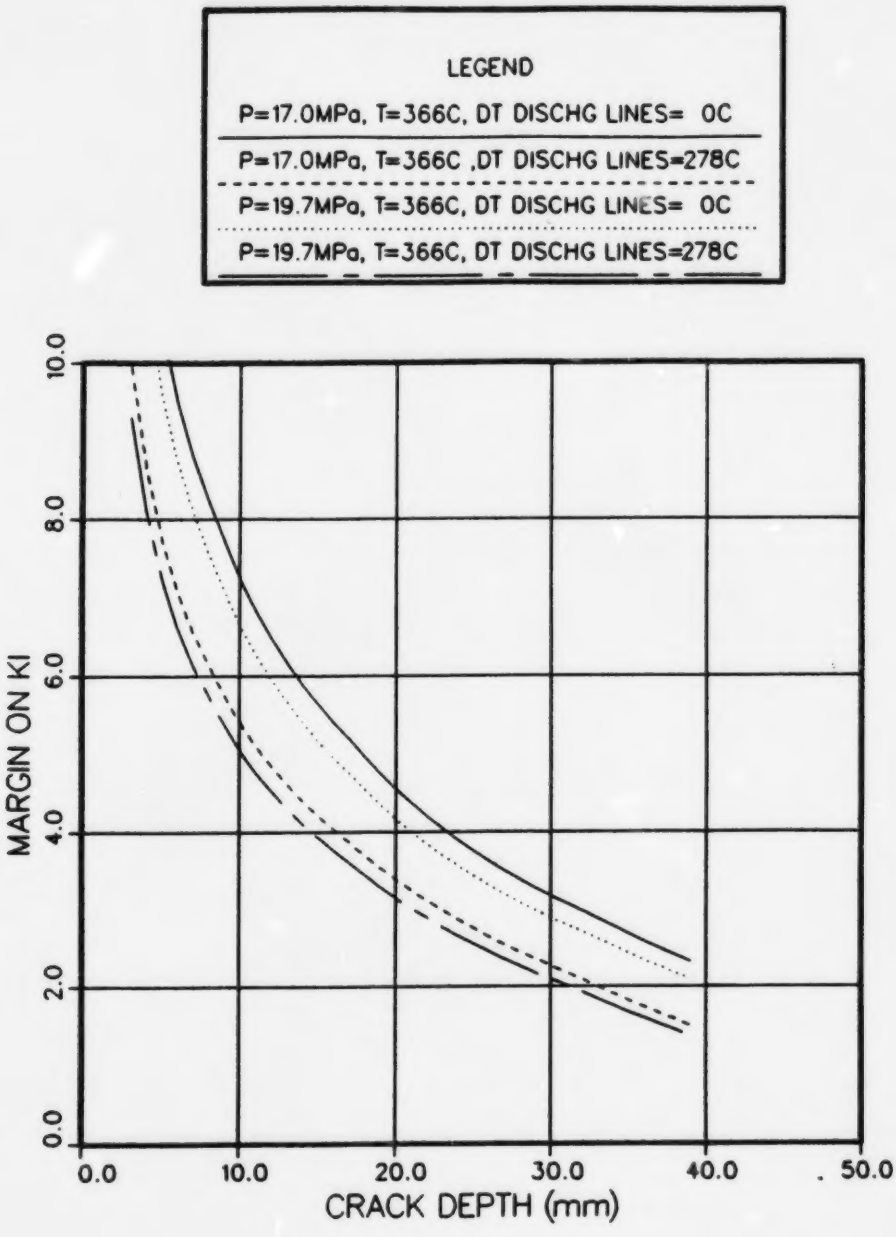


FIGURE 9-1
Variation of the margin on the crack-tip stress intensity factor with crack depth for an axisymmetric crack in the suction nozzle for normal operating and design pressures.

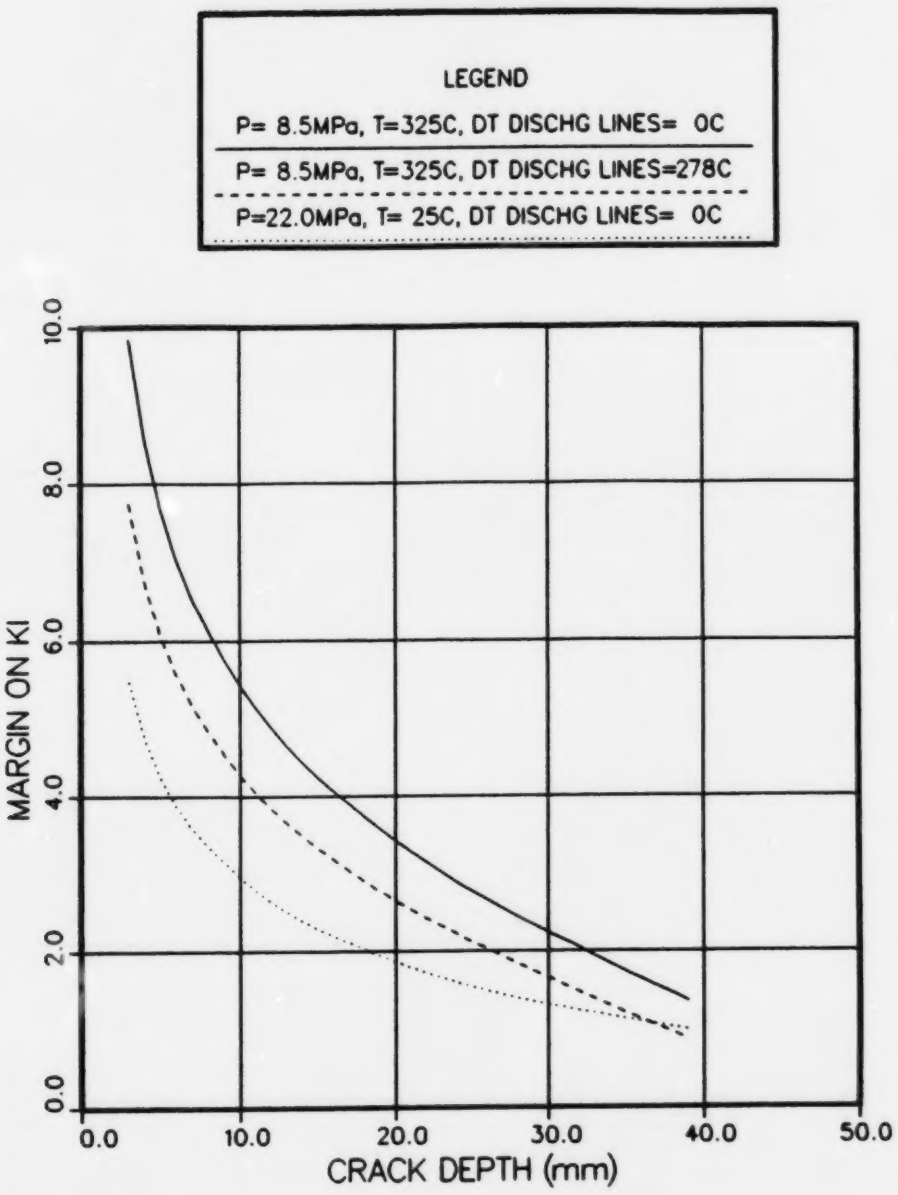


**FIGURE 9-2**
**Variation of the margin on the crack-tip stress intensity factor with crack depth for an axisymmetric crack in the suction nozzle for the cooldown transient and the hydrostatic test.**

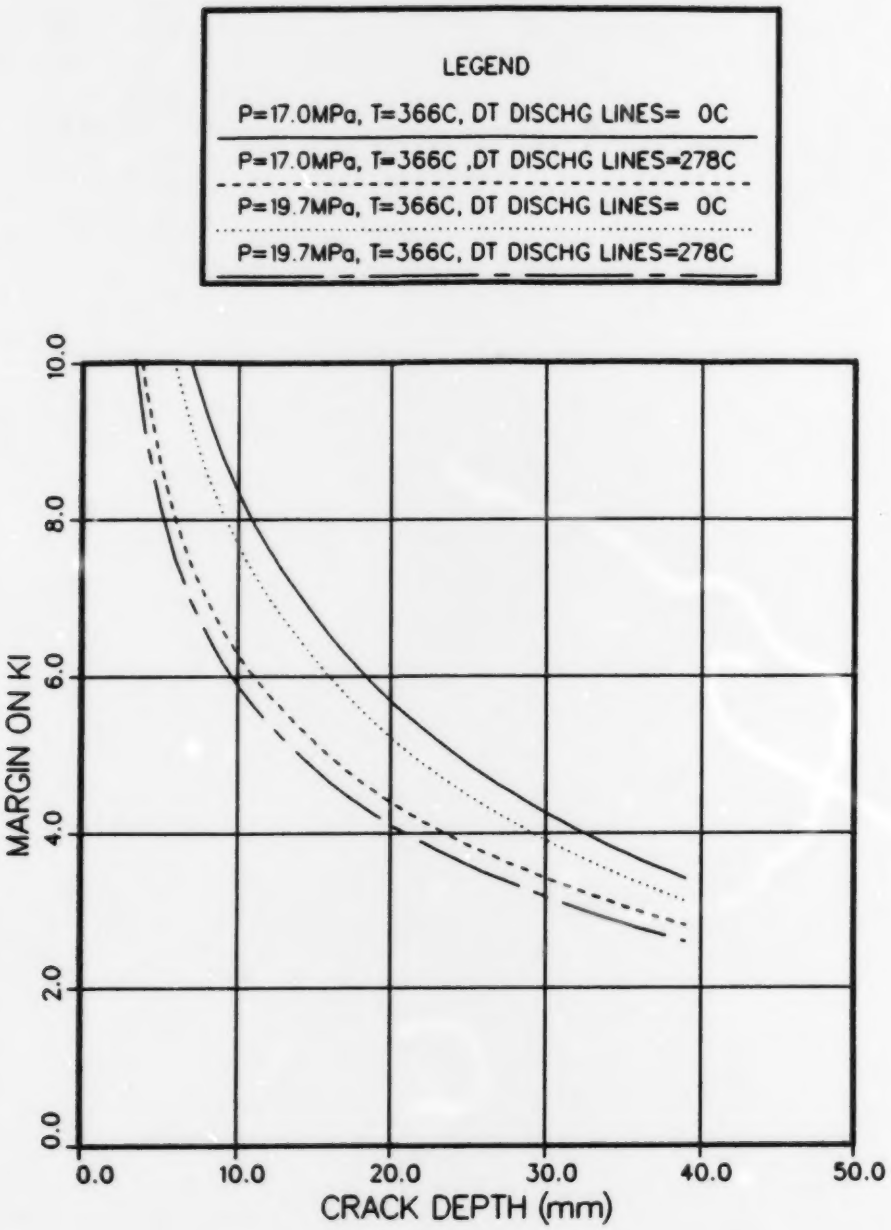


FIGURE 9-3
Variation of the margin on the crack-tip stress intensity factor with crack depth for a crack aspect ratio of 10 to 1 in the suction nozzle for normal operating and design pressures.

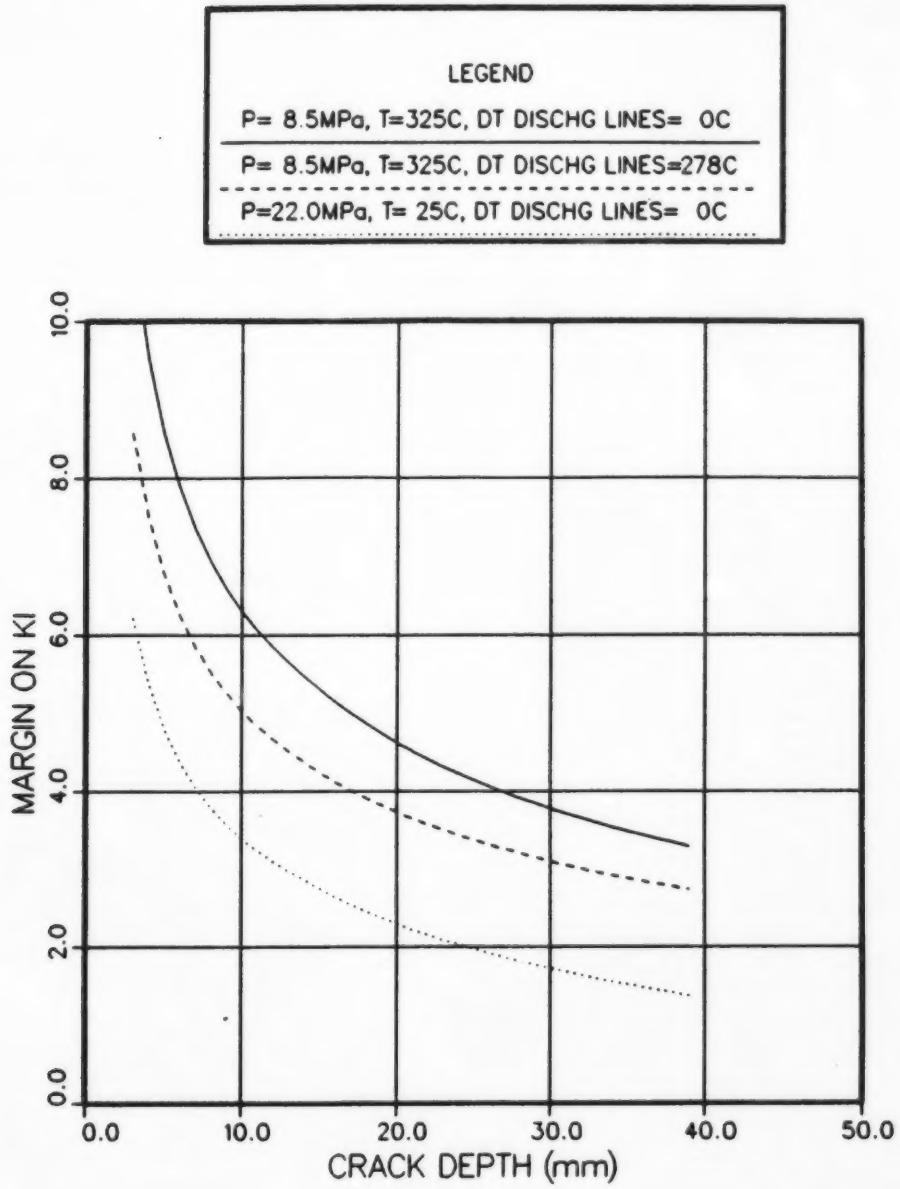


FIGURE 9-4
Variation of the margin on the crack-tip stress intensity factor with crack depth for a crack aspect ratio of 10 to 1 in the suction nozzle for the cooldown transient and the hydrostatic test.

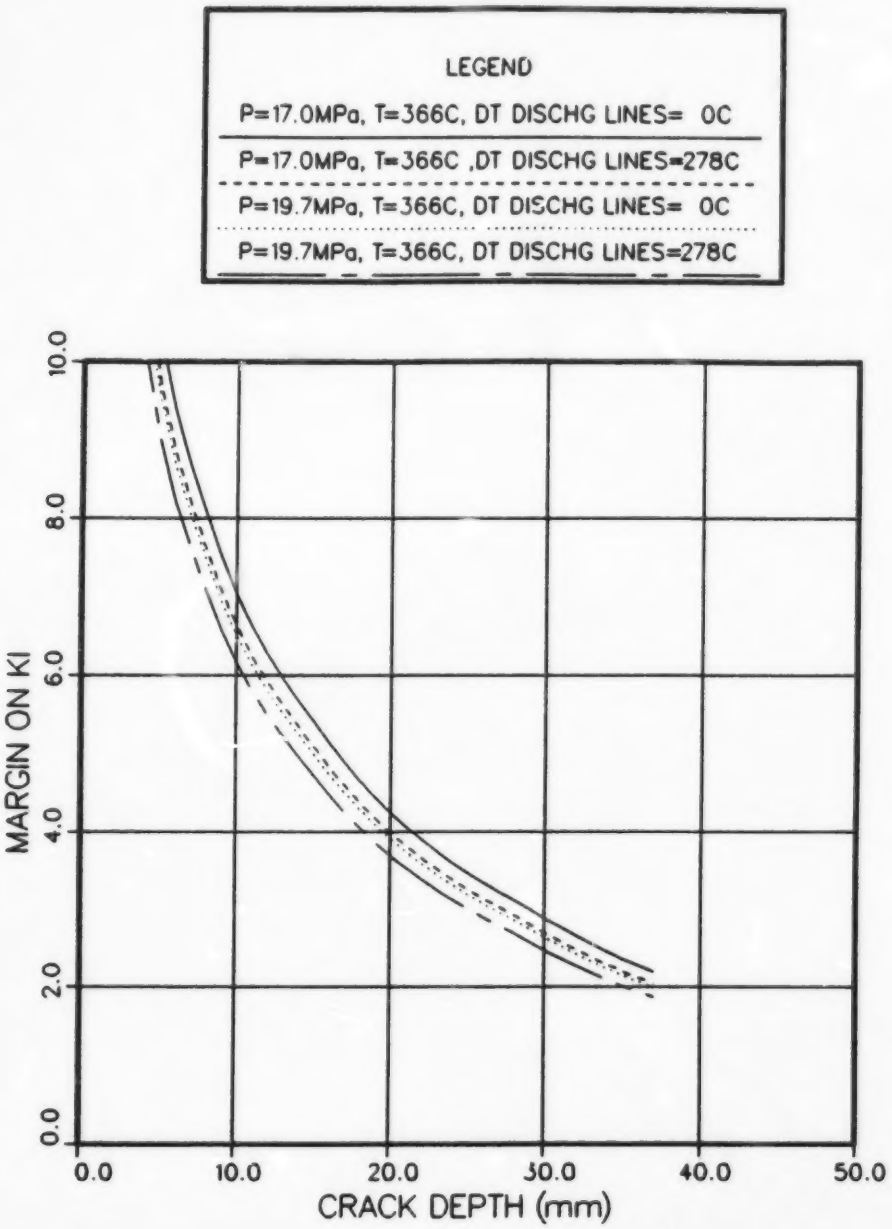


FIGURE 9-5
Variation of the margin on the crack-tip stress intensity factor with crack depth for an axisymmetric crack in the downcomer nozzle for normal operating and design pressures.

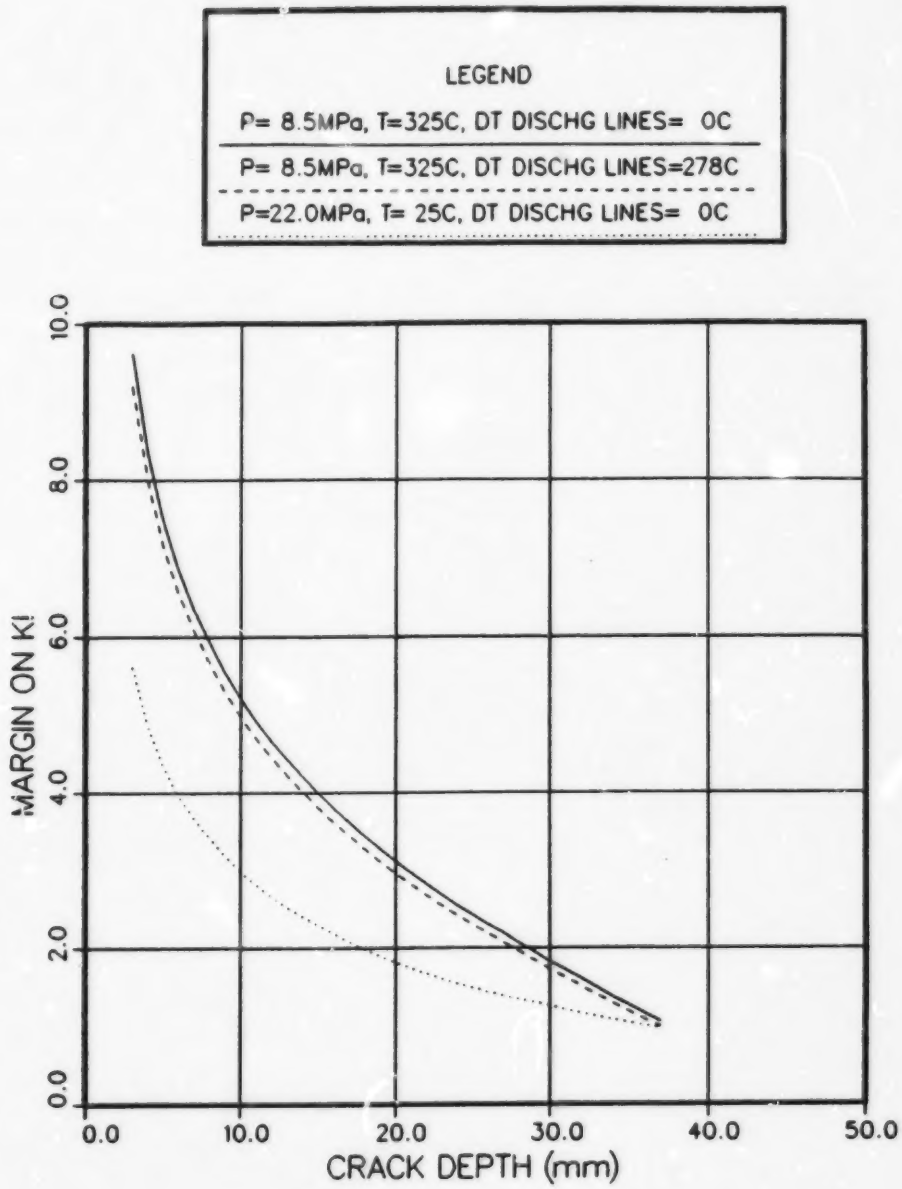


FIGURE 9-6
Variation of the margin on the crack-tip stress intensity factor with crack depth for an axisymmetric crack in the downcomer nozzle for the cooldown transient and the hydrostatic test.

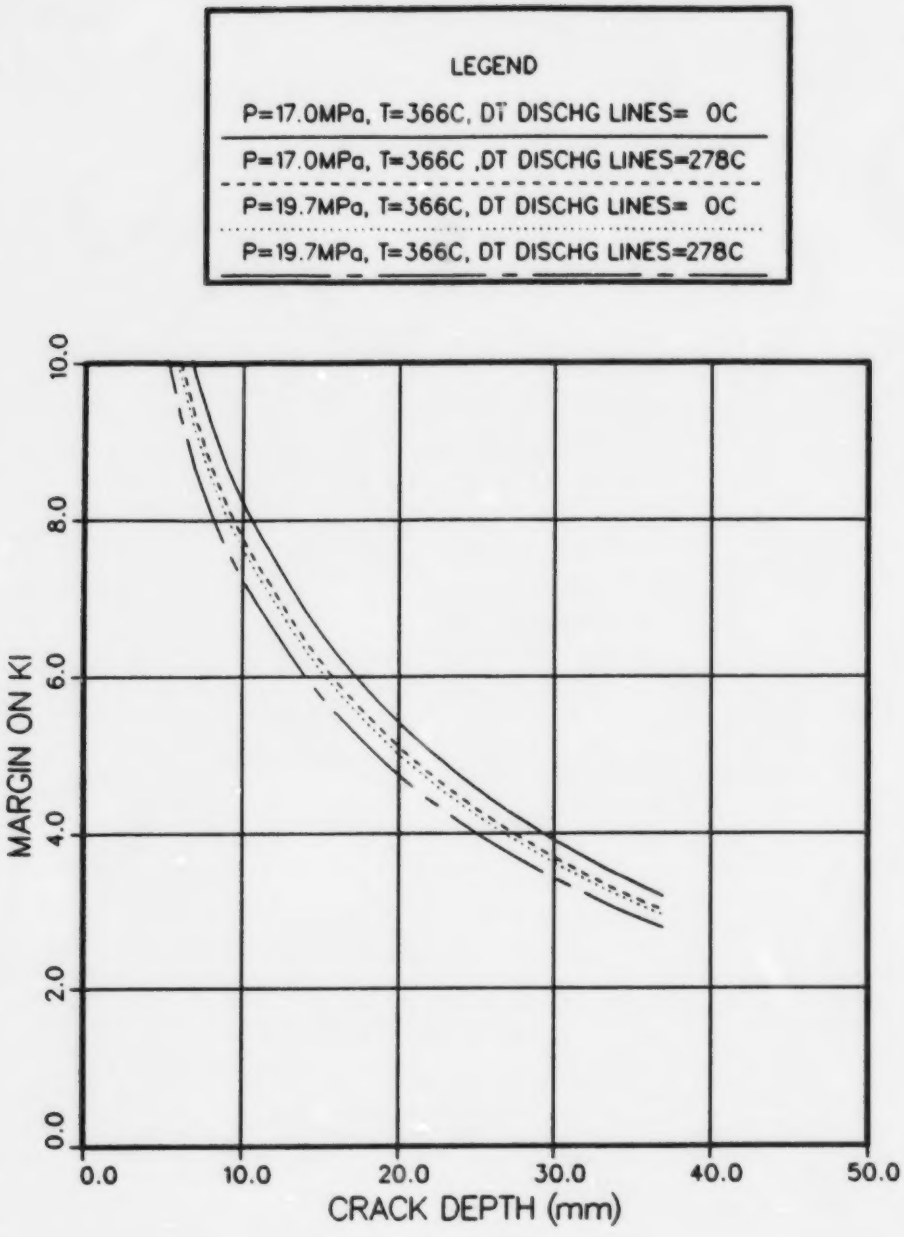


FIGURE 9-7
Variation of the margin on the crack-tip stress intensity factor with crack depth for a crack aspect ratio of 10 to 1 in the downcomer nozzle for normal operating and design pressures.

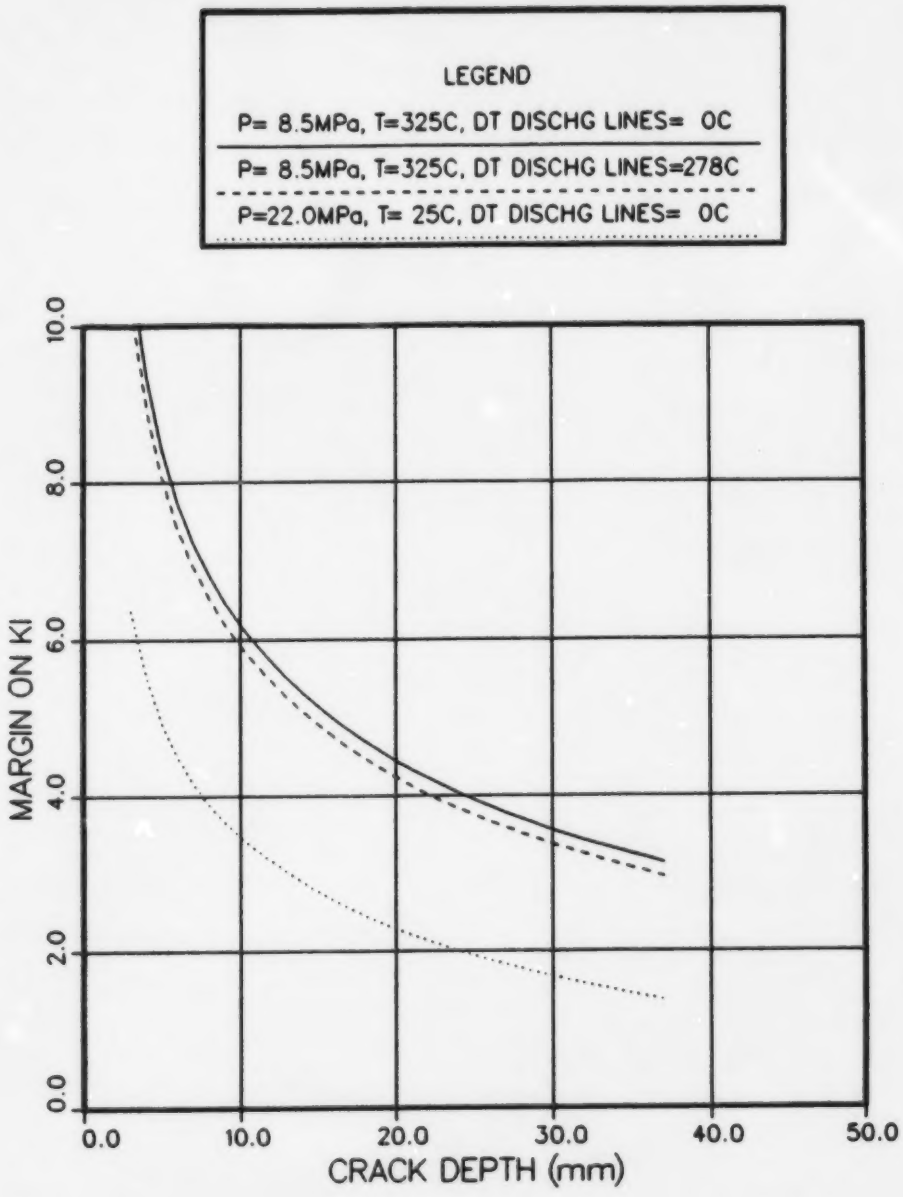


FIGURE 9-8
Variation of the margin on the crack-tip stress intensity factor with crack depth for a crack aspect ratio of 10 to 1 in the downcomer nozzle for the cooldown transient and the hydrostatic test.

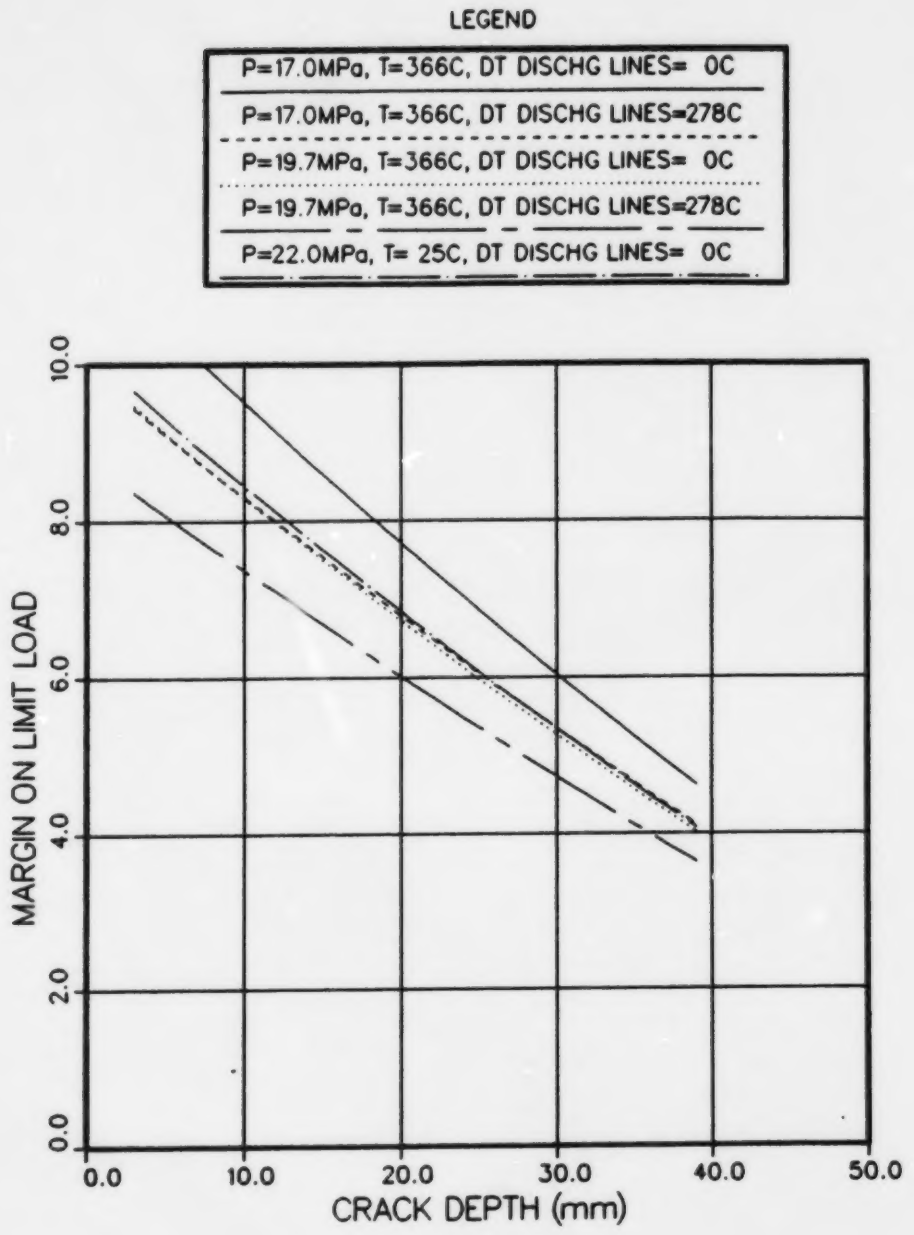


**FIGURE 9-9**
**Variation of the margin against plastic collapse with crack depth for an axisymmetric crack in the suction nozzle**

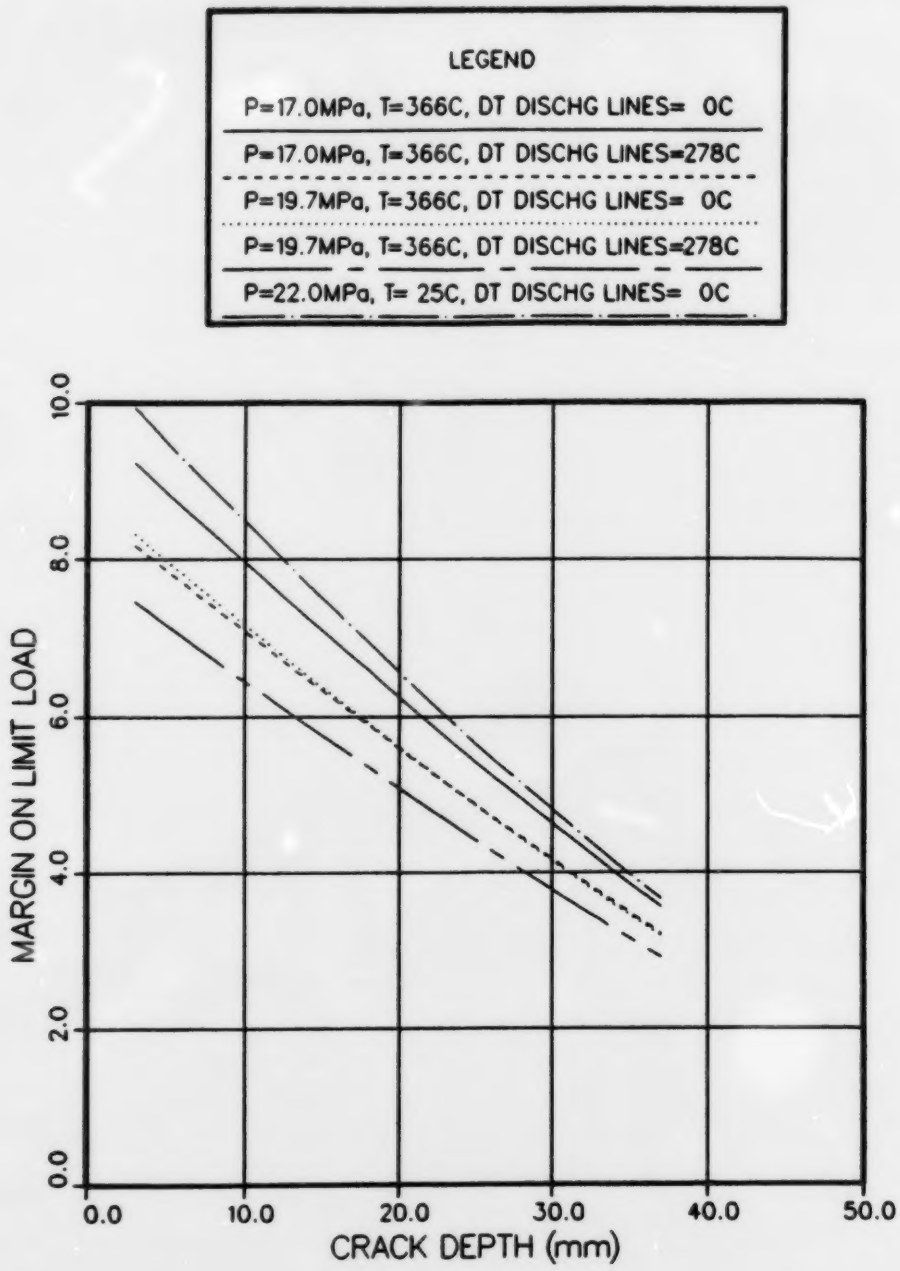


FIGURE 9-10
Variation of the margin against plastic collapse with crack depth for an axisymmetric crack in the downcomer nozzle.

## APPENDIX A

## Calculation of Stresses Due to Mechanical Loads

## APPENDIX A

### Calculation of Stresses Due to Mechanical Loads

The stresses were based on three-dimensional elastic finite element calculations performed by Wardrop Engineering Inc. /7/. Details of the Wardrop calculations can be obtained from the author of this report. The stresses from the Wardrop calculations for the various loads were scaled and combined by using linear superposition to determine the actual stresses. The engineering drawings are in imperial units (in., lbf, psi, etc.), and the finite element stress calculations were performed using these units. This appendix is also based on imperial units. Final stress values are also given in MPa. The finite element calculations were based on an assumed system temperature of 688°F.

### A-1 Calculation of Loads

This was Stage 1 as described in Section 5.1, and the reader is referred to read Section 5.0 of this report first. A schematic of the piping system modelled is given in Figures 5-1 and A-1. Information was obtained from engineering drawings as well as directly from CTS. The internal pressure loading included the axial force on the nozzle and suction manifold due to the closed-end effect on a pressurized cylinder. The deadweight load was estimated by summing the weight of the pump casing, pump motor, discharge lines and water, and applying the load as a vertical force $F_y$. The same force of 50,800 lbf was applied to the suction nozzle and the downcomer nozzle. The loads due to differential thermal expansion of the piping were calculated by using the commercial finite element computer code ANSYS. The analysis was elastic, and the pipe and pipe-fitting elements in ANSYS were used. The finite element model is shown as the schematic in Figures 5-1 and A-1. The loads which were used in the subsequent stress analysis were those loads which would induce stresses normal to the cracks. With reference to Figure A-1, these loads are the vertical force $F_y$, and the moments $M_x$ and $M_z$. Since the analysis was linear, arbitrary temperature differences between the waterwall tubes and the bulk of the piping, and between the off-line pump discharge lines and the bulk of the piping were used in the finite element calculations. Two calculations were performed based on the piping temperatures given in Table A-1. The boundary conditions were:

a) The upper ends of the waterwall tubes and downcomers were displaced by the piping expansion displacements shown on the engineering drawings.

b) The two outside pump discharge lines were each supported by a spring support with a stiffness of 2500 lbf/in.

The resultant forces and moments from the two calculations are given in Table A-2. The actual temperatures used for the two pump operation scenarios in the flaw evaluation are also given in Table A-1. The load sets given in Table A-2 were linearly scaled and combined to account for the actual piping temperature differences used in the flaw evaluation. By representing the load components $F_y$, $M_x$ and $M_z$ as L, the final load sets for the scenario of all pumps remaining on line were calculated by using:

$$L(T_{ww}\text{-}752^{\circ}F,\ T_{pc}\text{-}688^{\circ}F) = [(752\text{-}688)/(698\text{-}688)]\ L(T_{ww}\text{-}698^{\circ}F,\ T_{pc}\text{-}688^{\circ}F) \quad \text{(A-1)}$$

where $T_{ww}$ is the temperature of the waterwall tubes and $T_{pc}$ is the temperature of the two discharge lines for Pump C. The final load sets for the second scenario of Pump C being off-line were calculated by using

$$L(T_{ww}\text{-}752^{\circ}F,\ T_{pc}\text{-}188^{\circ}F) = L(T_{ww}\text{-}752^{\circ}F,\ T_{pc}\text{-}688^{\circ}F) + [(688\text{-}188)/(688\text{-}588)][L(T_{ww}\text{-}698^{\circ}F,\ T_{pc}\text{-}588^{\circ}F) - L(T_{ww}\text{-}698^{\circ}F,\ T_{pc}\text{-}688^{\circ}F)] \quad \text{(A-2)}$$

Due to the flexibility of the waterwall tubes the final loads were insensitive to temperature changes of the waterwall tubes. The maximum of the absolute value of each load component on each of the two types of nozzles for each scenario are given in Table A-3. For a given nozzle type, not all of the maximum loads acted on the same nozzle. In the flaw evaluation, it was conservatively assumed that all the maximum loads did act on one nozzle.

## A-2 Three-Dimensional Calculations of Stress Distributions in the Nozzles

This was Stage 2 of the analysis described in Section 5.1. Three-dimensional elastic finite element calculations of stresses in the suction manifold and nozzles assembly were performed by Wardrop Engineering Inc. by using the commercial finite element computer code ANSYS. The 8-noded brick solid element was employed. The purpose of these calculations was to obtain the stress concentration distributions in the tee region where a nozzle joins the suction manifold. Each loading component: pressure, $F_y$, $M_x$ and $M_z$ was applied in turn to each of the two nozzles. The stresses due to internal pressure, deadweight and the vertical force $F_y$ due to thermal expansion are symmetric across both axes of the horizontal cross-section of a nozzle (top portion of Figure 1-2). The stresses due to $M_x$ and $M_z$ are symmetric across one axis, and anti-symmetric (change sign) across the other axis. Therefore, one quadrant of a nozzle will have positive stresses due to each load component and will be the "worst case" quadrant in which all loads act in a positive sense. The variation of the through-wall stress distribution around the circumference of this quadrant was examined.

The vertical location of maximum stress was in the weldment, where the wall thickness is greater than in the nozzle itself. The through-wall stress distributions, which when combined result in the maximum for the "worst case" quadrant, are given for the suction nozzle in Figures A-2 to A-4. The conditions are the normal operating pressure of 2466 psi (17.0 MPa) with one pump off-line. The corresponding stress distributions for the downcomer nozzle are given in Figures A-5 to A-7. Also plotted are the linear idealizations of the stress distributions used in the flaw evaluation. The linear stress distributions were written as a membrane stress plus a pure through-wall bending stress, as illustrated in Figure 5-2. The normalized membrane and through-wall bending stresses for three circumferential locations around the "worst

case" quadrant in the suction nozzle are given in Table A-4. The angle theta is shown in Figure 1-2, where theta = 90° corresponds to point A. The normalization consisted of dividing the stress by the stress which would occur in a straight pipe under the same loads (F/A or $MR_o/I$). Also given in Table A-4 are the maximum normalized stresses for the "worst case" quadrant in the downcomer nozzle. Since the stresses in the downcomer nozzle are lower, the maximum stresses due to each load were simply added together regardless of circumferential position around the nozzle.

## A-3 Superposition of Stresses Due to Mechanical Loads

The loads given in Table A-3 were combined with the unit stress coefficients given in Table A-4 to calculate the circumferential variation in the "worst case" quadrant of total stress due to mechanical loads for the suction nozzle. The internal pressure was 2466 psi (17.0 MPa). The results for the scenario of one pump off-line are given in Table A-5. The maximum stresses for each load in the "worst case" quadrant for the downcomer nozzle are given in Table A-6. The maximum through-wall stress distributions for both nozzle types occurred at theta = 90° (point A in Figure 1-2) for both scenarios of all pumps on-line, and one pump off-line. In the flaw evaluation the maximum stresses at point A were conservatively idealized as being axisymmetric around the circumference of the nozzle. The welding residual stress and local thermal stress due to through-wall temperature gradients were also assumed to be axisymmetric.

TABLE A-1

Temperatures Used in Piping Thermal Expansion Analyses

| Component | Temperatures Used in Wardrop Piping Expansion Calculations (°F) | | Temperatures Used in Actual Flaw Evaluation (°F) | |
|---|---|---|---|---|
| | All Pumps On-Line | Pump C Off-Line | All Pumps On-Line | Pump C Off-Line |
| Discharge Lines for Pumps A, B, and D. | 688 | 688 | 688 | 688 |
| Pump C | 688 | 588 | 688 | 188 |
| Waterwall Tubes | 698 | 698 | 752 | 752 |
| Remainder of System | 688 | 688 | 688 | 688 |

TABLE A-2

Resultant Loads on the Nozzles
From the Wardrop Piping Expansion Calculations

| Nozzle | Loads for All Pumps On-Line | | | Loads for Pump C Off-Line | | |
|---|---|---|---|---|---|---|
| | $F_y$ (lbf) | $M_x$ (in-lbf) | $M_z$ (in-lbf) | $F_y$ (lbf) | $M_x$ (in-lbf) | $M_z$ (in-lbf) |
| Suction for: | | | | | | |
| Pump A | -787 | 26,220 | 25,025 | 1,175 | 80,807 | 238,047 |
| Pump B | -2,722 | -89,361 | 81,818 | 1,758 | 129,351 | 272,984 |
| Pump C | -2,722 | -89,361 | -81,818 | -16,789 | -742,234 | -562,004 |
| Pump D | -787 | 26,220 | -25,025 | 6,171 | 475,962 | 687,040 |
| Downcomer 2 | -513 | -15,242 | -21,247 | 1,005 | -5,043 | -22,222 |
| Downcomer 3 | -1,043 | -16,220 | -12,831 | 130 | -6,261 | -14,430 |
| Downcomer 4 | -1,588 | -16,619 | -2,839 | -3,255 | -9,344 | -7,039 |
| Downcomer 5 | -1,588 | -16,619 | 2,839 | -6,706 | -14,567 | 1,090 |
| Downcomer 6 | -1,043 | -16,220 | 12,831 | -3,327 | -12,946 | 17,518 |
| Downcomer 7 | -513 | -15,242 | 21,247 | 2,118 | -3,120 | 22,168 |

TABLE A-3

Final Loads on Nozzles Used in the Flaw Evaluation

| Nozzle | Loads for All Pumps On-Line | | | Loads for Pump C Off-Line | | |
|---|---|---|---|---|---|---|
| | $F_y$ (lbf) | $M_x$ (in-lbf) | $M_z$ (in-lbf) | $F_y$ (lbf) | $M_x$ (in-lbf) | $M_z$ (in-lbf) |
| Suction Nozzle | 17,421 | 571,910 | 523,635 | 87,756 | $3.8363 \times 10^6$ | $3.5353 \times 10^6$ |
| Downcomer Nozzle | 10,163 | 106,362 | 135,981 | 35,753 | 106,362 | 140,856 |

TABLE A-4

Normalized Membrane and
Through-Wall Bending Stresses in the Nozzles

| Normalized Stress | Suction Nozzle | | | Downcomer Nozzle |
|---|---|---|---|---|
| | Angle Theta+ | | | |
| | 0° | 45° | 90° | |
| Internal Pressure: | | | | |
| $\sigma_m/(p\pi R_i^2/A)$ | 1.9417 | 1.4523 | 1.5537 | 1.4582 |
| $\sigma_b/(p\pi R_i^2/A)$ | -2.3886 | 0.0 | 0.0 | 0.0 |
| Force $F_y$: | | | | |
| $\sigma_m/(F_y/A)$ | 1.7285 | 1.3581 | 0.5556 | 3.5030 |
| $\sigma_b/(F_y/A)$ | -1.3170 | -1.9446 | -1.5330 | 0.0 |
| Moment $M_x$: | | | | |
| $\sigma_m/(M_xR_o/I)$ | -0.9061 | -0.2255 | 0.1039 | 2.1588 |
| $\sigma_b/(M_xR_o/I)$ | 1.5401 | 1.0772 | 0.3798 | 0.0 |
| Moment $M_z$: | | | | |
| $\sigma_m/(M_zR_o/I)$ | 0.3772 | -0.5055 | 0.0160 | 0.5400 |
| $\sigma_b/(M_zR_o/I)$ | -0.2383 | 0.6070 | 0.6690 | 0.0 |

$A = \pi(R_o^2 - R_i^2)$

$I = (\pi/4)(R_o^4 - R_i^4)$

$R_i$ = inner radius

$R_o$ = outer radius

+ See Figure 1-2

TABLE A-5

Superposition of Stresses Due to
Mechanical Loads for the Suction Nozzle for One Pump Off-Line

| Load | Angle Theta+ | | | | | |
|---|---|---|---|---|---|---|
| | 0° | | 45° | | 90° | |
| | Membrane $\sigma_m$(psi) | Bending $\sigma_b$(psi) | Membrane $\sigma_m$(psi) | Bending $\sigma_b$(psi) | Membrane $\sigma_m$(psi) | Bending $\sigma_b$(psi) |
| Internal Pressure - 2,466 psi(17.0MPa) | 5,749 | -7,072 | 4,300 | 0.0 | 4,600 | 0.0 |
| Deadweight - 50,800 lbf | 526 | -344 | 409 | -593 | 170 | -500 |
| Piping Thermal Expansion Loads: | | | | | | |
| $F_y$=87,756 lbf | 878 | -669 | 690 | -988 | 282 | -779 |
| $M_x$=3.8363x$10^6$in-lbf | -4,734 | 8,047 | -1,178 | 5,629 | 543 | 1,985 |
| $M_z$=3.5353x$10^6$in-lbf | 1,816 | -1,147 | -2,434 | 2,923 | 77 | 3,221 |
| Total in psi | 4,235 | -1,185 | 1,787 | 6,971 | *5,672 | *3,927 |
| Total in MPa | 29.20 | 8.17 | 12.32 | 48.06 | 39.11 | 27.08 |

* Use maximum stresses at theta = 90°

\+ See Figure 1-2

TABLE A-6

Superposition of Stresses Due to
Mechanical Loads for the Downcomer Nozzle for One Pump Off-Line

| Load | Membrane $\sigma_m$(psi) | Bending $\sigma_b$(psi) |
|---|---|---|
| Internal Pressure - 2,466 psi (17.0 MPa) | 4,000 | 0.0 |
| Deadweight - 50,800 lbf | 720 | -640 |
| Piping Thermal Expansion Loads: | | |
| $F_y$ - 35,753 lbf | 1,040 | 0.0 |
| $M_x$ - 106,362 in-lbf | 555 | 0.0 |
| $M_z$ - 140,856 in-lbf | 184 | 0.0 |
| Total in psi | 6,499 | -640 |
| Total in MPa | 44.81 | 4.41 |

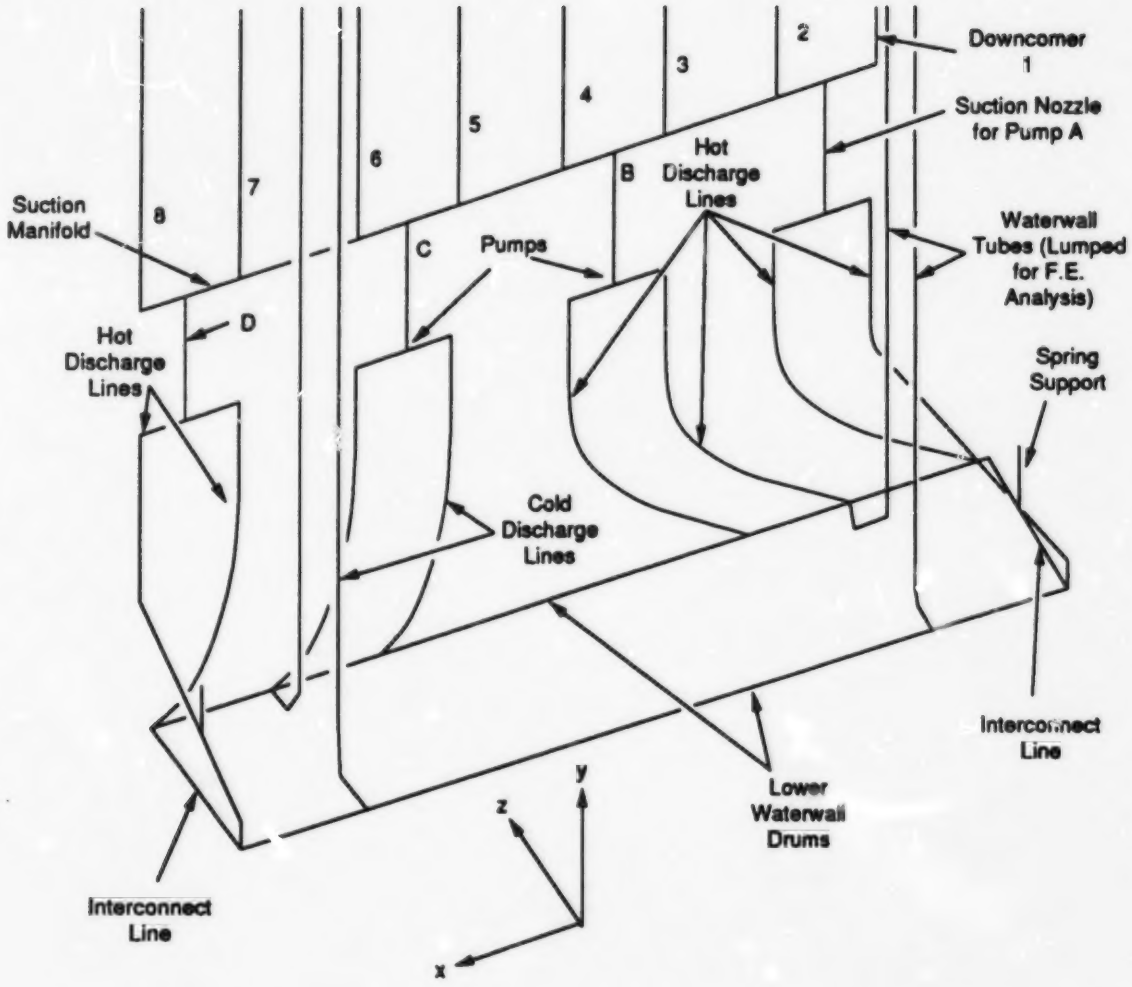


FIGURE A-1
Schematic of lower portion of piping system

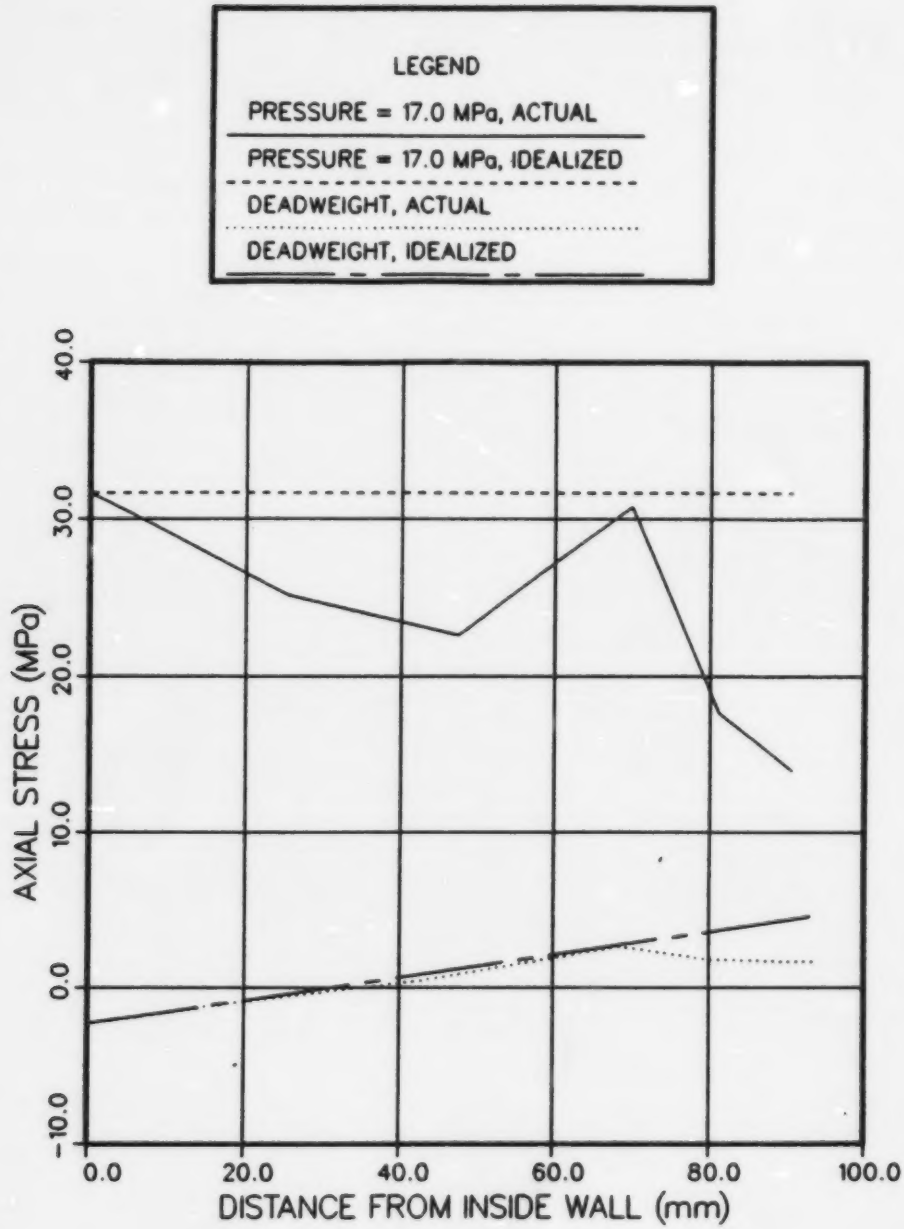


FIGURE A-2
Axial stress distribution through the wall thickness of the suction nozzle weldment used in the flaw evaluation for internal pressure and deadweight.

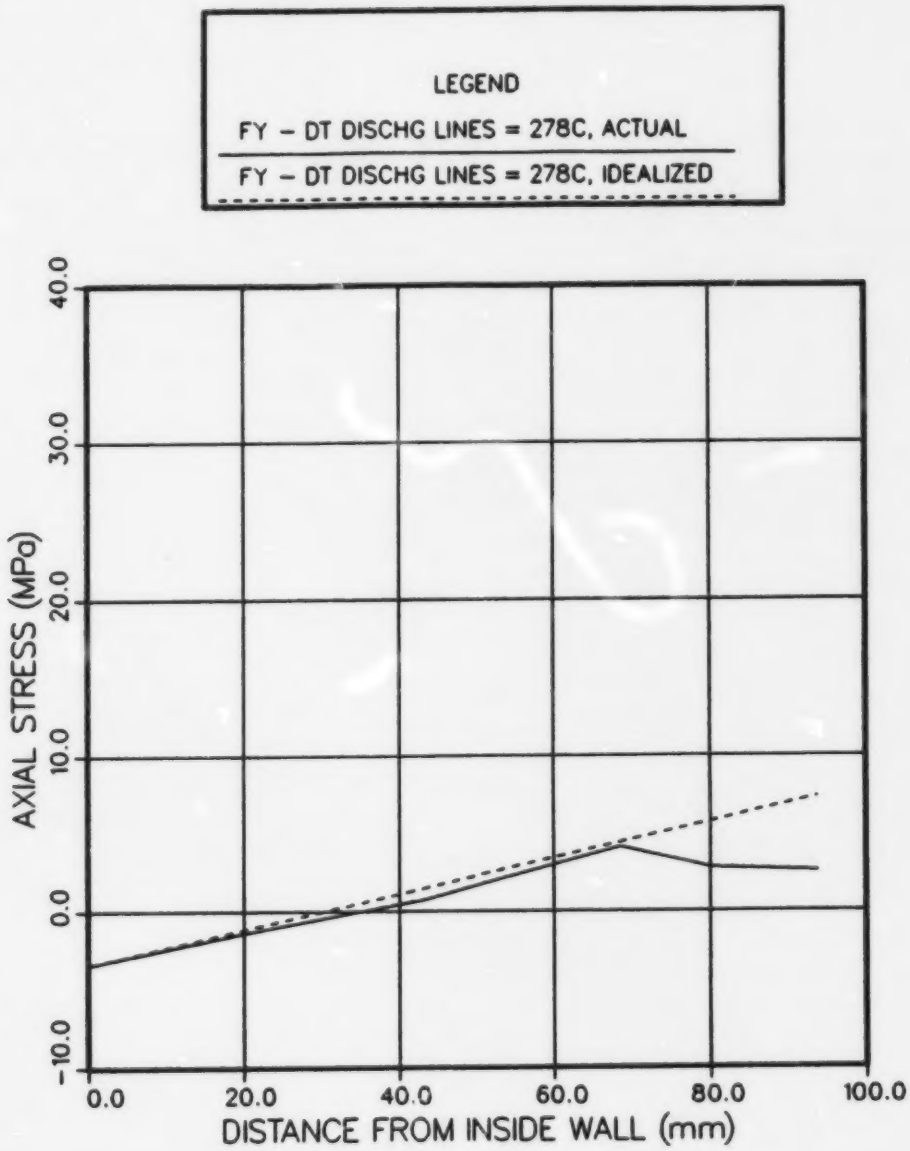


FIGURE A-3
Axial stress distribution through the wall thickness of the suction nozzle weldment used in the flaw evaluation for piping thermal expansion force-one pump off-line.

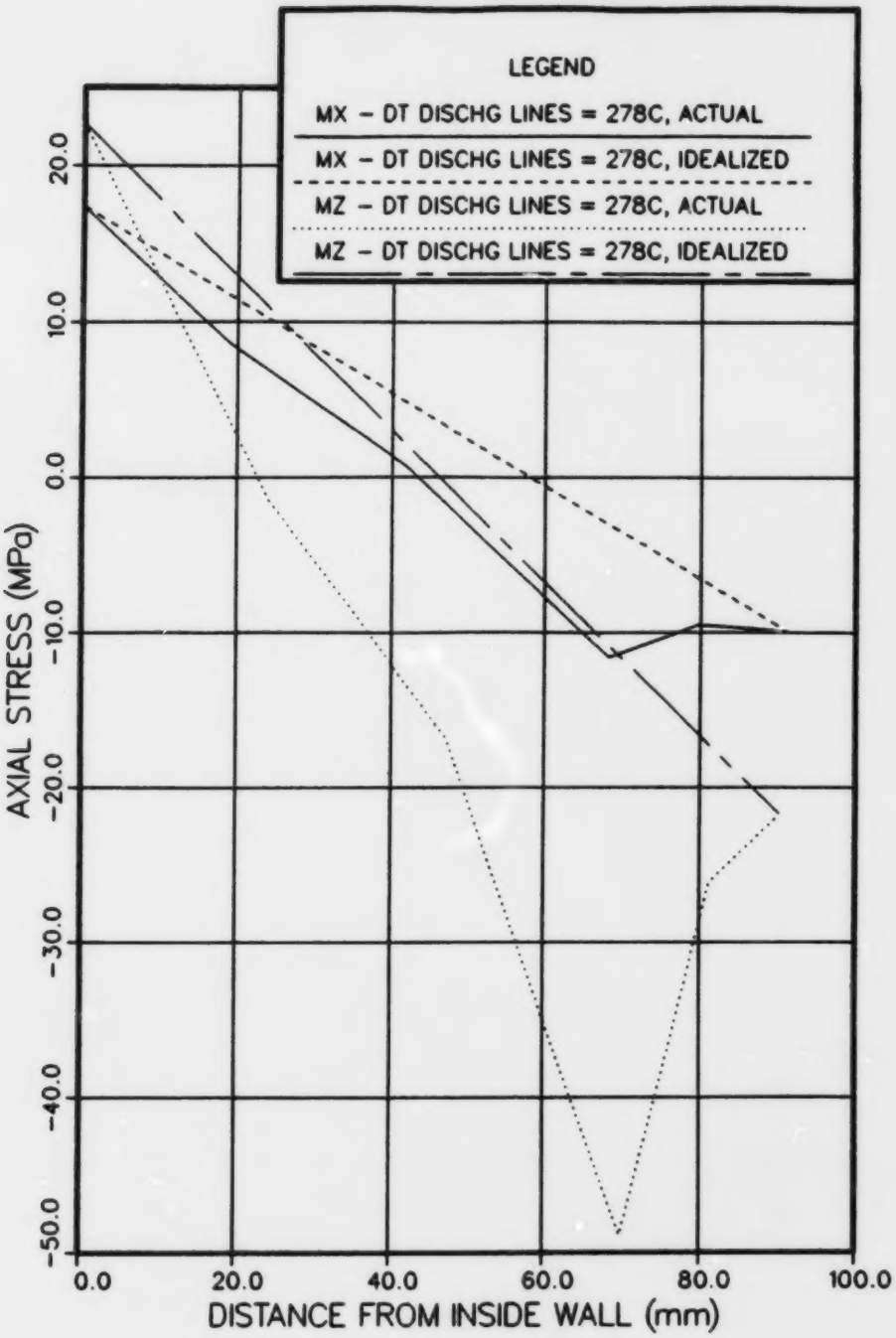


FIGURE A-4
Axial stress distribution through the wall thickness of the suction nozzle weldment used in the flaw evaluation for piping thermal expansion bending moments - one pump off-line.

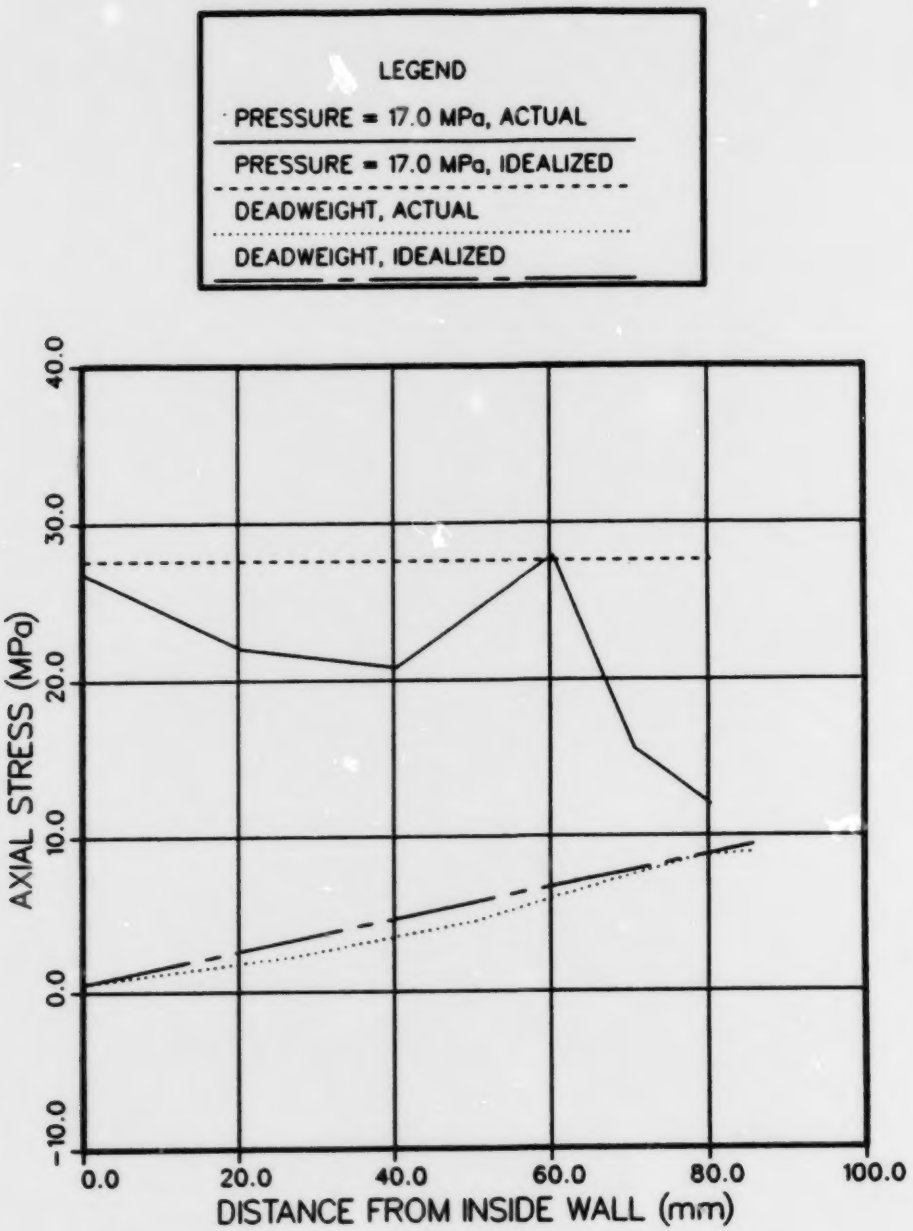


**FIGURE A-5**
**Axial stress distribution through the wall thickness of the downcomer nozzle weldment used in the flaw evaluation for internal pressure and deadweight.**

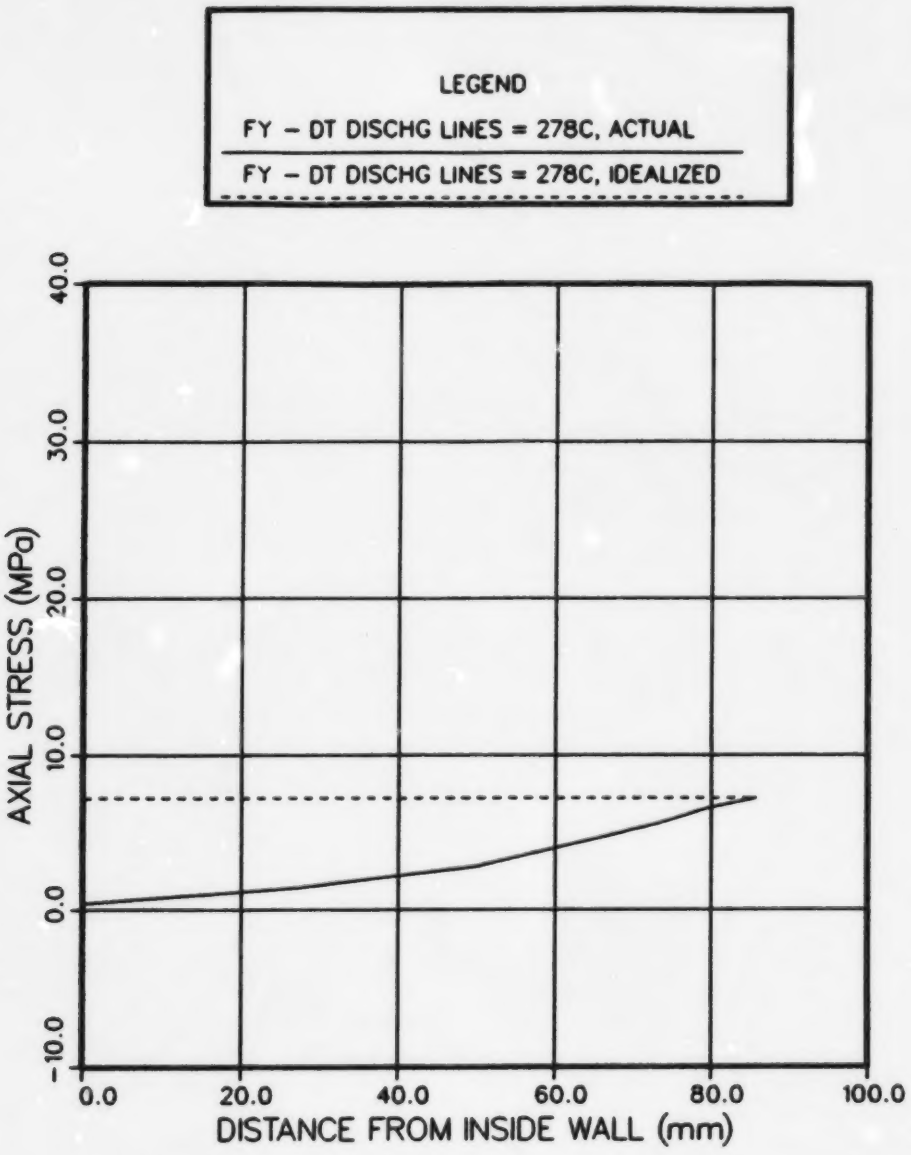


**FIGURE A-6**
**Axial stress distribution through the wall thickness of the downcomer nozzle weldment used in the flaw evaluation for piping thermal expansion force - one pump off-line.**

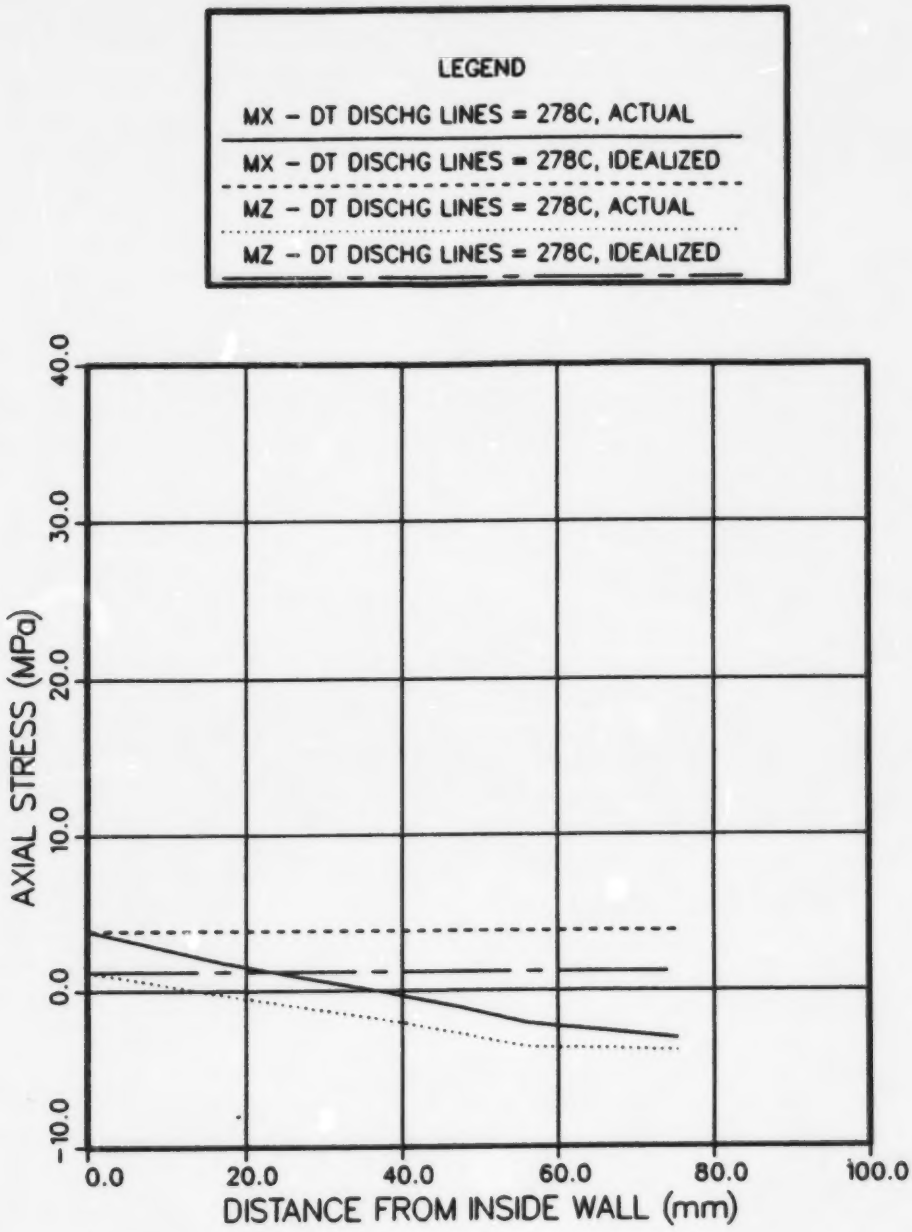


FIGURE A-7
Axial stress distribution through the wall thickness of the downcomer nozzle weldment used in the flaw evaluation for piping thermal expansion moments - one pump off-line.

## APPENDIX B

### Geometry Correction Factors For The Crack-Tip Stress Intensity Factor

## APPENDIX B

### Geometry Correction Factors For The Crack-Tip Stress Intensity Factor

### B-1 Axisymmetric Crack

The solution for the membrane stress geometry correction factor $F_m$ was taken from EPRI NP-1931/10/ and is given in Table B-1. The solution for the bending stress geometry correction factor $F_b$ was taken from Tada, Paris and Irwin/11/ and corresponds to a single edge-cracked plate under bending

$$F_b = 1.122 - 1.40\ (a/t) + 7.33\ (a/t)^2 - 13.08\ (a/t)^3 + 15.0\ (a/t)^4 \qquad \text{(B-1)}$$

where a is the crack depth and t is the wall thickness.

### B-2 Semi-Elliptical Crack

#### Membrane Stress Correction Factor - Deepest Point

The solution for the membrane stress geometry correction factor for the deepest point of crack penetration was taken from Zahoor/12/.

$$F_m = 1 + Q^2\ [0.02 + g(0.0103 + 0.00617\ g)] \qquad \text{(B-2)}$$

(deepest point)

where $Q = 1 + 1.464\ (a/c)^{1.65}$,

$c$ = one-half the crack length,

$g = (a/t)/(a/2c)$.

#### Membrane Stress Correction Factor - Surface Point, Bending Stress Correction Factors

Solutions for the membrane stress geometry correction factor for the intersection of the crack front with the free surface, and for the bending stress geometry correction factors were taken from Newman and Raju/13/ for a surface crack in a flat plate. The value of the geometry correction factor depends on the parametric angle $\phi$ around the crack front. In the formulae given below, $\phi = \pi/2$ corresponds to the deepest point of crack penetration, and $\phi = 0$ corresponds to the intersection of the crack front with the inside wall surface. The membrane stress correction factor is given by

$$F_m = f_1\ f_2\ [M_1 + M_2\ (a/t)^2 + M_3\ (a/t)^4] \qquad \text{(B-3)}$$

where $M_1 = 1.13 - 0.09\ (a/c)$

$$M_2 = -0.54 + 0.89/(0.2 + (a/c))$$

$$M_3 = 0.5 - 1.0/(0.65 + (a/c)) + 14\,(1.0 - (a/c))^{24}$$

$$f_1 = [(a/c)^2\,(\cos\phi)^2 + (\sin\phi)^2]^{0.25}$$

$$f_2 = 1 + (1.0 - \sin\phi)^2\,[0.1 + 0.35\,(a/t)^2]$$

The bending stress correction factor is given by

$$F_b = [H_1 + (H_2 - H_1)(\sin\phi)^v]\,F_m \qquad \text{(B-4)}$$

where $H_1 = 1 - 0.34\,(a/t) - 0.11\,(a/c)(a/t)$

$$H_2 = 1 + G_1\,(a/t) + G_2\,(a/t)^2$$

$$G_1 = -1.22 - 0.12\,(a/c)$$

$$G_2 = 0.55 - 1.05\,(a/c)^{0.75} + 0.47\,(a/c)^{1.5}$$

$$v = 0.2 + (a/c) + 0.6\,(a/t)$$

TABLE B-1

Membrane Stress Geometry Correction
Factor for the Axisymmetric Crack

| a/t | $F_m$ |
|---|---|
| 0.0 | 1.16 |
| 0.125 | 1.16 |
| 0.250 | 1.26 |
| 0.500 | 1.61 |
| 0.750 | 2.15 |